








A genome-wide in vivo CRISPR screen identifies essential regulators of T cell migration to the CNS in a multiple sclerosis model

Received: 28 September 2022

Accepted: 14 August 2023

Published online: 14 September 2023

 Check for updates

Arek Kendirli ^{1,2,6}, Clara de la Rosa^{1,2,3,6}, Katrin F. Lämmle ^{1,2,6}, Klara Eglseer^{1,2}, Isabel J. Bauer^{1,2}, Vladyslav Kavaka^{1,2}, Stephan Winklmeier ^{1,2}, La Zhuo^{1,2}, Christian Wichmann⁴, Lisa Ann Gerdes^{1,2,5}, Tania Kümpfel^{1,2}, Klaus Dornmair ^{1,2}, Eduardo Beltrán ^{1,2,5}, Martin Kerschensteiner ^{1,2,5,7} ✉ & Naoto Kawakami ^{1,2,7} ✉

Multiple sclerosis (MS) involves the infiltration of autoreactive T cells into the CNS, yet we lack a comprehensive understanding of the signaling pathways that regulate this process. Here, we conducted a genome-wide in vivo CRISPR screen in a rat MS model and identified 5 essential brakes and 18 essential facilitators of T cell migration to the CNS. While the transcription factor ETS1 limits entry to the CNS by controlling T cell responsiveness, three functional modules, centered around the adhesion molecule $\alpha 4$ -integrin, the chemokine receptor CXCR3 and the GRK2 kinase, are required for CNS migration of autoreactive CD4⁺ T cells. Single-cell analysis of T cells from individuals with MS confirmed that the expression of these essential regulators correlates with the propensity of CD4⁺ T cells to reach the CNS. Our data thus reveal key regulators of the fundamental step in the induction of MS lesions.

MS is the most common disabling neurological disease in young adults. In MS, the cascade of tissue injury is initiated when activated autoreactive T cells infiltrate the CNS^{1–3}. The importance of this step in MS pathogenesis is well evidenced from studies in rodent models of the disease and in humans. The capacity of CD4⁺ T cells to induce CNS inflammation has, for example, been demonstrated in rodent experimental autoimmune encephalomyelitis (EAE) models, in which activated T cells recognizing myelin basic protein (MBP) are transferred into naïve rodents where they induce an MS-like disease⁴. Experiments

in such models have delineated the migratory path of encephalitogenic T cells to the CNS⁵; uncovered the compartments and cellular interactions that shape the induction of CNS inflammation^{6,7} and aided in the identification of adhesion molecules, such as $\alpha 4$ -integrin, that are required for T cell migration to the CNS^{6,8}. Clinical data have confirmed the importance of these processes in individuals with MS, showing that many of the gene loci conferring increased risk of the disease are predicted to affect CD4⁺ T cell activation and differentiation⁹; that there is an MS-associated immune gene signature in a subset of CD4⁺ T cells in

¹Institute of Clinical Neuroimmunology, University Hospital, Ludwig-Maximilians-Universität München, Munich, Germany. ²Biomedical Center (BMC), Faculty of Medicine, Ludwig-Maximilians-Universität München, Martinsried, Germany. ³Graduate School of Systemic Neurosciences, Ludwig-Maximilians-Universität München, Munich, Germany. ⁴Division of Transfusion Medicine, Cell Therapeutics and Haemostaseology, University Hospital, Ludwig-Maximilians-Universität München, Munich, Germany. ⁵Munich Cluster for Systems Neurology (SyNergy), Munich, Germany.

⁶These authors contributed equally: Arek Kendirli, Clara de la Rosa, Katrin F. Lämmle. ⁷These authors jointly supervised this work: Martin Kerschensteiner, Naoto Kawakami. ✉e-mail: martin.kerschensteiner@med.uni-muenchen.de; naoto.kawakami@med.uni-muenchen.de

monozygotic twins discordant for the disease¹⁰; that CD4⁺ T cells start colonizing the CNS from early stages of the disease¹¹; and that therapies targeting T cell migration can be effective in ameliorating MS¹².

Despite significant advances in our understanding of MS and how to treat it, most studies to date have focused on assessing and validating the roles of molecules known to be involved in T cell trafficking. However, this has left key knowledge gaps in the field, and we lack a comprehensive understanding of the essential molecular cues and signaling streams that enable or limit T cell entry to the CNS and may thus represent alternative targets for therapy. The advent of CRISPR gene editing technology now raises the possibility of conducting comprehensive and unbiased loss-of-function screens in disease models in vivo: indeed genome-wide CRISPR screens have been successfully used to answer questions related to cancer initiation, propagation and therapy^{13,14}, as well as to reveal the mechanisms regulating critical immunological processes including T cell activation, proliferation and fate determination^{15–17}. To date, this powerful approach has not been applied to study the initiation of CNS inflammation.

Here we used a rodent MS model and combined an unbiased genome-wide CRISPR screen with functional in vivo validation studies, multiphoton microscopy and in vitro mechanistic experiments, to provide a definite molecular characterization of the central step in MS pathogenesis, the infiltration of autoreactive T cells to the CNS.

Results

CRISPR screen identifies essential regulators of T cell migration to the CNS

To study the molecular regulation of autoreactive T cell trafficking to the CNS in MS, we used a rat EAE model, in which an MS-like disease is induced by the transfer of MBP-reactive T (T_{MBP}) cells^{4,7,18}. We first conducted a genome-wide screen to identify candidate molecules whose deletion significantly enhanced or impaired T_{MBP} cell migration into the CNS. We transduced T_{MBP} cells in a first step with the Cas9 nuclease and enhanced green fluorescent protein (EGFP), and then with blue fluorescent protein (BFP) and a genome-wide CRISPR library containing 87,690 single guide RNAs (sgRNAs) targeting 21,410 genes and 396 microRNAs (miRNAs), as well as 800 non-targeting (NT) control sgRNAs. We included 300×10^6 T cells per replicate transduced at a multiplicity of infection (MOI) < 0.3 so that statistically most T cells would contain no more than one sgRNA¹⁹, each different sgRNA would be present in about 1,000 T cells (1,000× coverage) and each gene would be targeted by four different sgRNAs. After 6 d, these cells were injected intravenously into naïve Lewis rats. Three days later, at the time of first EAE symptoms, we isolated T cells from the blood, spleen, spinal cord meninges and parenchyma (Fig. 1a) and used next-generation sequencing (NGS) followed by bioinformatic analysis with the MAGeCK software²⁰ to compare the sgRNA distribution for each gene between each of the peripheral and CNS compartments (Fig. 1b). To the list of genes showing a differential distribution between compartments, we applied a set of selection criteria based on effect size and statistical significance (Methods and Supplementary Table 1), leading to the identification of 1,961 candidate target genes for a subsequent validation

screen. *Itga4*, which encodes the target of the therapeutic monoclonal antibody natalizumab, $\alpha 4$ -integrin, was one of the most-depleted genes in all comparisons of peripheral compartments versus the CNS (Fig. 1b), validating the ability of this approach to identify clinically relevant molecules. Furthermore, we found that many of the same genes appeared to regulate the entry of autoreactive T cells to both the meninges and the spinal cord parenchyma in EAE (Extended Data Fig. 1).

In a validation screen, we repeated the adoptive transfer experiment for the 1,961 candidate gene targets identified in the genome-wide screen, but this time targeted more stringently with 6 sgRNAs per gene and with stricter selection criteria at the data analysis stage (for details, see Methods and Supplementary Table 2). Based on the relative fold change of the differential distribution and its robustness across sgRNAs and different compartments, we identified 18 essential ‘facilitators’ that are required for autoreactive T cell migration to the CNS (Fig. 1c,d) and 5 essential ‘brakes’ that limit T cell trafficking to the CNS (Fig. 1e,f). In contrast, none of the miRNAs fulfilled these criteria, indicating that no single miRNA is essential for either promoting or preventing T cell entry to the CNS (Extended Data Fig. 2). Furthermore, our approach also identified genes that differentially regulated the distribution of CD4⁺ T cells within the central (meninges versus spinal cord parenchyma) or peripheral (spleen versus blood) compartments; however, most of the genes involved showed comparably moderate fold changes (Extended Data Fig. 3).

The top-ranked hits of the 18 essential facilitators of CD4⁺ T cell entry to the CNS belonged to the Gene Ontology (GO) terms related to ‘adhesion molecules’ (most prominently *Itga4* and the functionally related *Fermt3* gene; Fig. 1g), ‘chemokine receptors’ (in particular *Cxcr3*; Fig. 1h) and ‘G-protein-coupled receptor (GPCR)-related proteins’ (such as *Grk2* and *Gnai2*; Fig. 1i). Notably, some of the essential genes also encoded transcriptional regulators (Fig. 1d) including: *Cbfb*, which has so far been primarily implicated in T cell differentiation²¹; *Tbx21*/T-bet, which controls genes important for the function of the $T_{\text{H}}1$ subset of helper T cells²²; *Foxo1*, encoding a prominent regulator of metabolic T cell fitness²³; and *Prdm1*, which is critical for both regulatory and cytotoxic T cell properties^{24,25}. Only one essential regulator, *Ska3*, which encodes a component of the microtubule-binding SKA1 complex²⁶, has a direct link to the cytoskeleton, indicating that most of the genes identified in our screen do not encode proteins that limit T cell mobility in general, but rather selectively impede trafficking from peripheral to CNS compartments.

The adhesion module: ITGA4, FERMT3 and HSP90B1

To further characterize the ‘adhesion module’, we first validated the effects of *Itga4*-knockout (KO) on T cell migration by CRISPR editing. We co-transferred *Itga4*-KO T_{MBP} cells expressing EGFP with T_{MBP} cells edited with a NT control sgRNA and expressing BFP (control T_{MBP} cells) into rats and collected cells from the blood and spinal cord meninges and parenchyma 3 d later (Fig. 2a). By flow cytometry, we confirmed that *Itga4* deletion significantly reduced T_{MBP} cell migration into the rodent CNS (Fig. 2b,c). Accordingly, the transfer of *Itga4*-KO T_{MBP} cells alone failed to induce disease symptoms in the recipient rats, while rats that received control T_{MBP} cells showed the expected disease course (Fig. 2a,d).

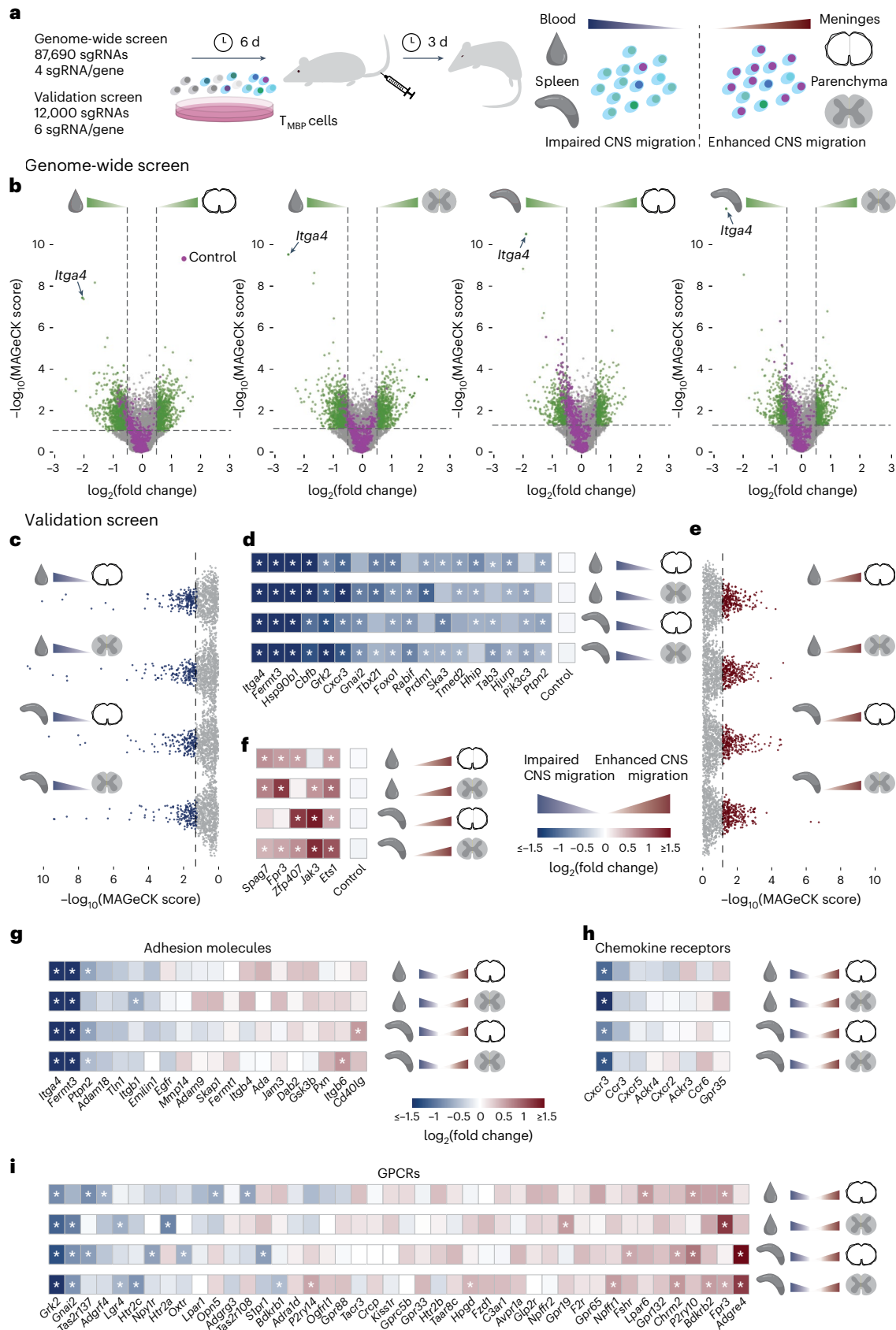
Fig. 1 | Genome-wide CRISPR screen identifies genes essential for autoreactive T cell migration to the CNS.

a, Experimental design. T_{MBP} cells were transduced in vitro with the genome-wide or validation CRISPR libraries, positively selected, reactivated and injected intravenously into Lewis rats. After 3 d, at disease onset, they were collected from blood, spleen, spinal cord meninges and parenchyma for analysis. **b**, Volcano plots depicting the genome-wide screen results per gene across four tissue comparisons. Green dots represent genes whose KO showed a sizeable change in the ability of T_{MBP} cells to migrate into the CNS. Lilac dots indicate controls. Lines at P value = 0.05 and $\log_2(\text{fold change}) = \pm 0.5$. **c–f**, Validation screen results showing the top-ranking genes whose KO showed impaired (c) or enhanced (e) migration into the CNS, across comparisons, and $\log_2(\text{fold change})$ heat maps showing the genes

essential for ‘facilitating’ T_{MBP} cell entry into the CNS (KO impairs migration, blue) (d) or for ‘braking’ CNS migration (KO enhances migration, red) (f). Essential candidates were defined as detailed in the Methods. **g–i**, $\log_2(\text{fold change})$ heat maps depicting the effects of gene KOs on T_{MBP} cells migration in the validation screen for adhesion-related genes (g) (GO terms GO.0050901, GO.0033631 and GO.0005178), chemokine receptors (h) (GO.0004950) and GPCRs (i) (GO.0004930, GO.0004703, GO.0001664 and guanine nucleotide-binding genes of GO.0001664, excluding genes present in GO.0004950 or GO.0004896). For **g–i**, only genes of the GO term with a P value < 0.05 (g and h) or P < 0.01 (i) and ≥ 3 ‘neg/pos|goodsgRNA’ per the validation screen results are shown. Asterisks indicate, for all heat maps: P value < 0.05, absolute $\log_2(\text{fold change}) > 3$ standard deviations of the $\log_2(\text{fold change})$ of the controls and ≥ 3 ‘neg/pos|goodsgRNA’.

Considering other adhesion-related genes that might work alongside *Itga4* to drive T cell migration into the CNS, we next assessed the effects of knocking-out *Hsp90b1*. The HSP90 heat shock protein family has been proposed to act as chaperones and allow correct folding of

integrins²⁷. Here we now show that one member, HSP90B1, in particular is essential for $\alpha4$ -integrin actions as *Hsp90b1*-KO T_{MBP} cells displayed a marked reduction of $\alpha4$ -integrin surface expression as well as a moderate reduction of the surface expression of $\beta1$ -integrin



and the lymphocyte function associated-antigen 1 (LFA-1) components α L-integrin and β 2-integrin (Fig. 2e) compared to control T_{MBP} cells. The moderate effects of HSP90B1 on β 1-integrin expression might be secondary to the reduced surface presence of α 4-integrin as the deletion of *Itga4* also reduced the expression of its binding partner β 1-integrin, while it did not result in marked changes of α L-integrin and β 2-integrin surface expression (Extended Data Fig. 4). Notably, this chaperone function of HSP90B1 appears to be conserved in humans, as CRISPR editing of HSP90B1 in human $CD4^+$ T cells isolated from peripheral blood resulted in a marked reduction of the surface expression of $CD49d/\alpha$ 4-integrin (Extended Data Fig. 4). In line with the marked effects of HSP90B1 on α 4-integrin surface expression, we observed a moderate yet significant reduction in T cell trafficking to spinal cord meninges and parenchyma (Fig. 2f,g), and a significantly milder EAE course (Fig. 2h) when *Hsp90b1*-KO T_{MBP} cells were transferred into rats. Like *Itga4*-KO T_{MBP} cells, *Hsp90b1*-KO T_{MBP} cells did not show altered expression of activation markers or the cytokines interferon (IFN)- γ and interleukin (IL)-17A (Extended Data Fig. 4).

Taken together, these results outline the functional T cell adhesion module that contains α 4-integrin, its intracellular binding partner kindlin3 (encoded by *Fermt3*, identified in our validation screen and with an established role in the intracellular activation of integrins²⁸), and its chaperone HSP90B1 (Fig. 2i). Notably, all other adhesion-related genes in our screen are nonessential (at least by our strict definition) and even deletion of *Itgb1* that encodes β 1-integrin, which pairs with α 4-integrin to form VLA-4, the binding partner for endothelial VCAM-1, shows only a mild reduction in T cell migration to the CNS, likely because it can be replaced by other β -integrins such as β 7-integrin²⁹.

The chemotaxis module: CXCR3, GNAI2 and TBX21

CXCR3, the receptor for CXCL9, CXCL10 and CXCL11, was the only top hit in our screen among the chemokine receptor family, despite previous work implicating both CXCR3 and CCR5 as regulators of T cell trafficking in the leptomeninges⁷. We first confirmed the essential role of CXCR3, showing that *Cxcr3*-KO T_{MBP} cells but not *Ccr5*-KO T_{MBP} cells migrated significantly less to the spinal cord meninges and parenchyma compared to co-transferred control T_{MBP} cells (Fig. 3a,b and Extended Data Fig. 5). Accordingly, transfer of *Cxcr3*-KO T_{MBP} cells induced significantly milder disease than did control T_{MBP} cells (Fig. 3c). This effect is likely related to the altered migratory capacities of these cells as *Cxcr3*-KO T_{MBP} cells did not show significant changes in the expression of adhesion molecules, activation markers or the cytokines IFN- γ and IL-17A (Extended Data Fig. 5).

Further analysis of this 'chemotaxis module' suggests that, in addition to CXCR3, two key proteins might be involved in chemoattraction of T cells into the CNS: the guanine nucleotide-binding protein GNAI2, which is linked to the intracellular transduction of signals induced by the CXCL9, CXCL10 and CXCL11 chemokines³⁰ and TBX21/T-BET, which controls the expression of the CXCR3 receptor²². To assess the role of GNAI2 in CXCR3-mediated migration, we compared the migration of

Cxcr3-KO and *Gnai2*-KO T_{MBP} cells to control T_{MBP} cells in a transwell chemotaxis assay. We found that *Cxcr3*-KO T cells showed altered transmigration in response to the CXCR3 ligand CXCL10, but not to the unrelated chemokine CCL5, while *Gnai2*-KO reduced migration toward both chemokines (Fig. 3d-f). This indicates that GNAI2 transduces the effects of CXCR3 on T cell migration and indeed we observed that *Gnai2*-KO T_{MBP} cells showed impaired migration to meninges and spinal cord parenchyma after transfer (Extended Data Fig. 5). Furthermore, CRISPR editing of the transcriptional regulator TBX21/T-BET in rat T_{MBP} cells and human $CD4^+$ T cells confirmed its critical role for controlling CXCR3 expression, which is conserved across species (Extended Data Fig. 5). Thus, based on these analyses, the chemotaxis module comprises CXCR3, GNAI2 and the transcription factor TBX21/T-BET (Fig. 3g).

The egress module: GRK2 controls T cell trafficking via S1PR1

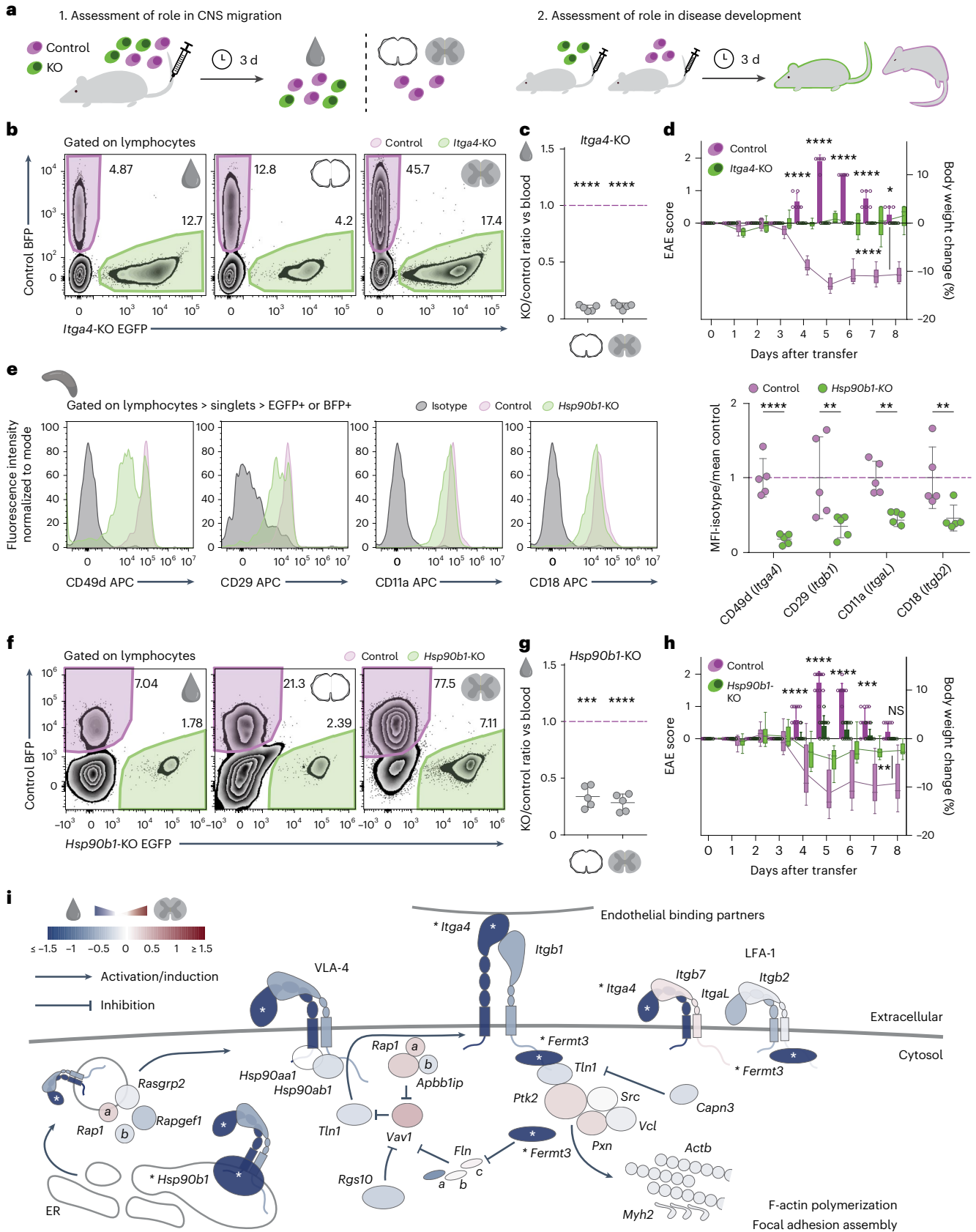
Among the GPCR-related proteins, the GPCR kinase 2 (GRK2) is the dominant hit in our screen with one of strongest effect sizes of any regulator outside the adhesion module (Fig. 1d,i). This was unexpected as GRK2 haploinsufficiency in mice had been previously related to an earlier disease onset in the EAE model³¹. Here we now established the essential role of GRK2 for CNS migration by transferring CRISPR-edited *Grk2*-KO T_{MBP} cells, which showed a significant reduction in their capacity to reach either spinal cord meninges or parenchyma (Fig. 4a,b), and induced significantly milder disease symptoms (Fig. 4c), compared to control T_{MBP} cells. As GRK2 has multiple potential target substrates and mechanisms³², we next asked which aspect of the transmigration process was affected by loss of GRK2. We performed in vivo multiphoton imaging of the rat spine after co-injection of *Grk2*-KO T_{MBP} cells expressing EGFP and control T_{MBP} cells expressing BFP (Fig. 4d). By tracking the location and movement of individual GRK2-deficient and GRK2-competent autoreactive T cells in the meninges, we found that GRK2 loss primarily affects the distribution of T cells between the intravascular and extravascular CNS compartments (Fig. 4e,f and Supplementary Movies 1 and 2), while the speed and the path lengths of crawling T cells along the vascular surface were mostly unaffected (Fig. 4g). Together with our observation that *Grk2*-KO T_{MBP} cells showed neither alterations in the expression of adhesion molecules, activation markers or the cytokines IFN- γ and IL-17A nor marked changes of their transcriptomic profile (Extended Data Fig. 6), this argues that loss of GRK2 alters the responsiveness of T cells to signals that determine their diapedesis but does not affect either their adhesion to the endothelial cells or their overall activation status or movement properties. These results are reminiscent of the altered trafficking of GRK2-deficient B cells between blood and lymph nodes that has been related to the desensitization of the S1PR1 receptors by GRK2 (ref. 33). Therefore, we next asked whether this mechanism was also important for T cell migration to the CNS using co-transfer experiments (Fig. 4h). We found that, while *Grk2*-KO T cells showed a marked impairment in trafficking from blood to either CNS compartment, these deficits were ameliorated

Fig. 2 | Functional validation of the adhesion module. **a**, Experimental design. KO-EGFP⁺ T_{MBP} cells were (1) co-transferred with control-BFP⁺ T_{MBP} cells or (2) transferred alone. (1) The relative proportions of control and KO cells in blood and CNS tissues were assessed by flow cytometry 3 d after transfer or (2) the animals were kept longer to assess disease development. **b,f**, Representative flow cytometry plots of T_{MBP} cells from blood, meninges and parenchyma after co-transfer with control and *Itga4*-KO (**b**) or *Hsp90b1*-KO (**f**) cells. **c,g**, Migratory phenotype of *Itga4*-KO (**c**) or *Hsp90b1*-KO (**g**) cells compared to control, shown as the ratio of KO to control T_{MBP} cells in meninges (left) or parenchyma (right) normalized to the KO/control ratio in blood. $n = 5$ rats. **d,h**, EAE score (bars) and weight changes (line) of control and *Itga4*-KO (**d**) or *Hsp90b1*-KO (**h**) injected animals; $n = 6$ rats per group for **d** and $n = 12$ control, $n = 11$ KO rats for **h**. **e**, Representative flow cytometry plots of integrin surface stainings of *Hsp90b1*-KO and control T_{MBP} cells isolated from the spleens of co-transferred rats 3 d after transfer; gray indicates isotype control, lilac indicates control, and green

indicates KO. Right, quantification of the median fluorescence intensity (MFI) with isotype background subtraction normalized to the mean control intensity. $n = 5$ rats. **i**, Schematic of the adhesion module with genes color coded based on the parenchyma versus blood comparison. Asterisks indicate significance across at least three pairwise tissue comparisons (Methods). **c,g**, One-sample *t*-test against hypothetical mean = 1; **d,h**, bars and dots, EAE score; box-and-whiskers plot and line, body weight change; repeated-measures two-way analysis of variance (ANOVA; days 3–8 for disease score; **d**, $F = 1094$, $P < 0.0001$; **h**, $F = 154.6$, $P < 0.0001$, and days 0–8 for weight changes; **d**, $F = 100.3$, $P < 0.0001$; **h**, $F = 11.89$, $P = 0.0024$) and Sidak's multiple-comparison test only for EAE score; **e**, two-way ANOVA ($F = 51.13$, $P < 0.0001$) with multiple comparisons with the two-stage linear step-up procedure of Benjamini, Krieger and Yekutieli. Figures show the mean \pm s.d. Not significant (NS), $P > 0.05$, * $P < 0.05$, ** $P < 0.01$, *** $P < 0.001$, **** $P < 0.0001$.

if T cells lacked both *Grk2* and *Slpr1* (Fig. 4i). As trafficking from the blood to CNS was unaltered in T_{MBP} cells deficient for *Slpr1* alone (Fig. 4i), these findings demonstrate that the essential contribution of GRK2 to the CNS entry of T cells is mediated via S1PR1 (Fig. 4j).

To assess whether this S1PR1–GRK2 axis is similarly operative in human T cells, we used CRISPR-edited human CD4⁺ T cells isolated from the peripheral blood of healthy donors (Fig. 5a). Our results demonstrate that human T cells lacking GRK2 showed partially impaired



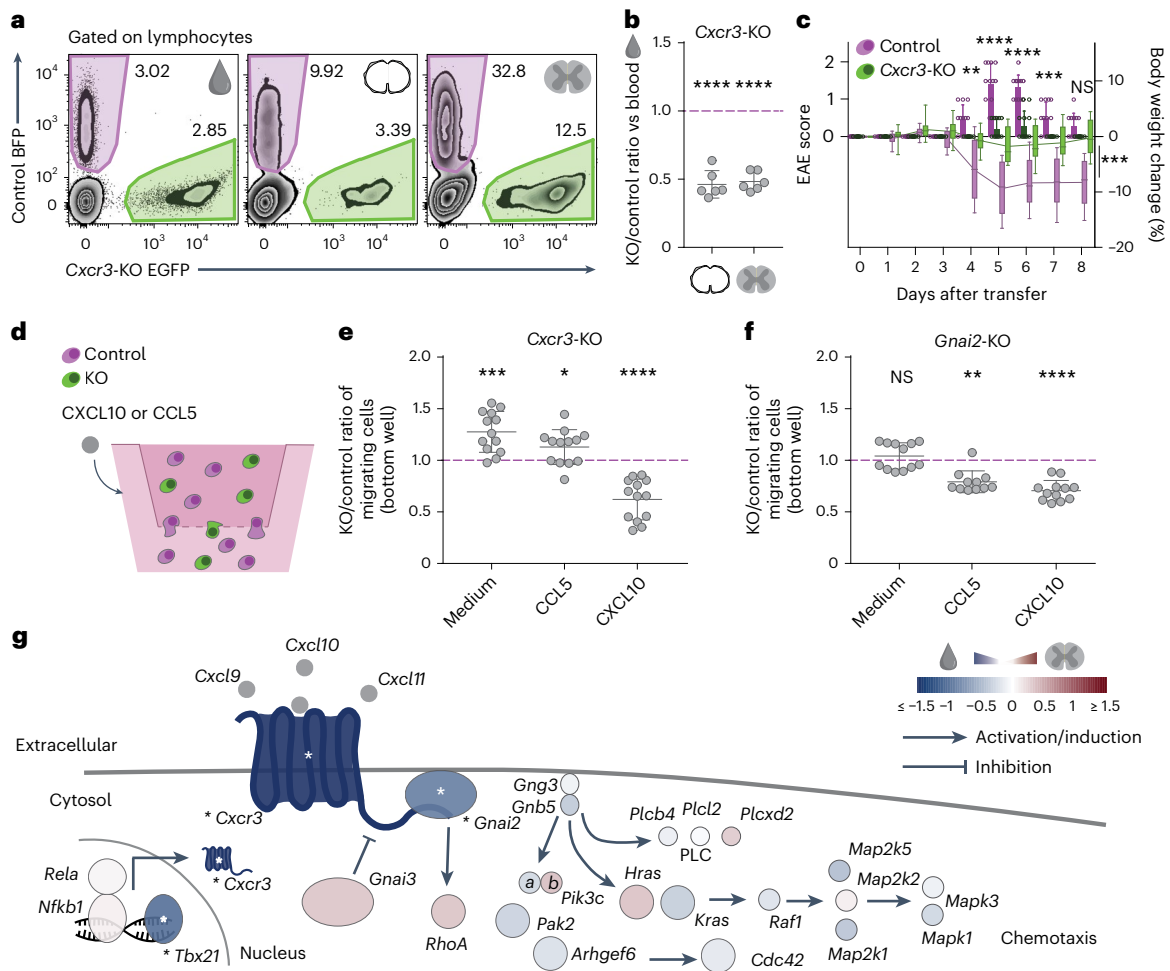


Fig. 3 | Functional validation of the chemotaxis module. a, Representative flow cytometry plots of T cells from blood, meninges and parenchyma after a co-transfer experiment with control and *Cxcr3*-KO cells. **b**, Migratory phenotype of *Cxcr3*-KO cells compared to control, shown as the ratio of KO and control T_{MBP} cells in meninges (left) or parenchyma (right) normalized to the KO/control ratio in blood. *n* = 6 rats. **c**, EAE score (bars) and weight changes (line) of control and *Cxcr3*-KO injected animals; *n* = 12 rats per group. **d**, Experimental design of in vitro transwell T_{MBP} cell migration experiments. Cells were seeded in the top chamber with medium, and control medium or chemokines were added to the bottom chamber. **e, f**, In vitro migration in response to chemokine gradient of *Cxcr3*-KO (**e**) cells and *Gnai2*-KO (**f**) cells normalized to control. *n* = 13 transwell

assays for *Cxcr3*-KO; *n* = 12 for *Gnai2*-KO medium and CXCL10; *n* = 11 for *Gnai2*-KO CCL5. **g**, Schematic of the CNS chemotaxis module centered around CXCR3. Genes are color coded based on the CRISPR screen phenotype in the parenchyma versus blood comparison. Asterisks indicate significance across at least three pairwise tissue comparisons (Methods). **b, e, f**, One-sample *t*-test or Wilcoxon signed-rank test against hypothetical mean = 1; **c**, bars and dots, EAE score; box-and-whiskers plot and line, body weight change; repeated-measures two-way ANOVA (days 3–8 for disease score ($F = 111.5, P < 0.0001$) and days 0–8 for weight changes ($F = 18.22, P = 0.0003$)) and Sidak’s multiple-comparison test only for EAE score. Figures show the mean \pm s.d. NS, $P > 0.05$, * $P < 0.05$, ** $P < 0.01$, *** $P < 0.001$, **** $P < 0.0001$.

internalization of S1PR1 in response to both S1P and fingolimod exposure (Fig. 5b,c). Furthermore, when we assessed the effects of GRK2 on the downstream signaling of S1PR1, we observed that the absence of GRK2 resulted in an excessive phosphorylation of ERK1/ERK2 (ref. 34) in response to S1P stimulation (Fig. 5d).

Taken together, these data delineate a third functional module that controls the egress of T cells by shifting the balance of attraction between blood and the CNS. This module is centered around the GRK2-mediated phosphorylation of S1PR1, which is likely induced by prolonged exposure of T cells to the S1P ligand in the blood, resulting in desensitization and subsequent internalization of S1PR1 (Fig. 4j). Our results indicate that *Grk2*-KO T cells are unable to egress from the blood even though they still receive attractive signals from the CNS, can adhere to the endothelium and can move inside blood vessels. Remarkably, the actions of S1PR1 agonists, effective therapeutic interventions in MS, also result in impaired S1PR1 signaling³⁵. In individuals treated with these agonists, however, it is assumed that

the failure of T cells to respond to S1P-mediated attraction to blood sequesters these cells in peripheral lymphoid tissues before they can even reach the CNS. Here too, *S1pr1*-KO did not affect the distribution of T_{MBP} cells between blood and CNS compartments (Fig. 4i) but led to an accumulation of these cells in the spleen (*S1pr1*-KO/control ratio in spleen versus blood of 1.37 ± 0.25 (s.d.), $P = 0.0291, n = 5$ rats; Extended Data Fig. 3) and parathymic lymph nodes (*S1pr1*-KO/control ratio in lymph nodes versus blood of 5.60 ± 3.24 (s.d.), $P = 0.0336, n = 5$ rats). Thus, our findings reveal the delicate regulatory balance that governs S1PR1 signaling during T cell trafficking, with either sustained blocking of signal transmission (as achieved by S1PR1 agonists) or a failure to curb signal transmission (as induced by GRK2 deficiency) preventing encephalitogenic T cells from entering the CNS.

ETS1 controls responsiveness of autoreactive T cells

In addition to the genes that facilitate CD4⁺ T cell entry to the CNS, our screen also detected five essential regulators, the loss of which

resulted in enhanced T cell trafficking to the spinal cord meninges and parenchyma. The top-ranked hit among these brakes of endogenous CNS migration was the transcriptional regulator ETS1, which regulates differentiation, survival and proliferation of lymphoid cells³⁶, and limits pathogenic T cell responses in atopic and autoimmune reactions^{37,38}. To validate the role of ETS1 in T cell migration into the CNS, we again used CRISPR editing to delete this gene in T_{MBP} cells and then co-transferred *Ets1*-KO and control cells into rats and assessed their trafficking. This confirmed that *Ets1* deletion results in increased trafficking to both meninges and parenchyma (Fig. 6a,b). Subsequent transcriptional analysis of *Ets1*-KO $CD4^+$ T cells isolated from the CNS compartment showed that these cells were likely to be more responsive to cytokine signals, and showed greater expression of genes encoding proinflammatory and cytotoxic mediators including IL-17, TNFRSF9, NKG7 and PRF1 (Fig. 6c–f), the expression levels of some of which were also increased in human *Ets1*-KO $CD4^+$ T cells (Fig. 6g,h). In rats, this hyperresponsive and proinflammatory transcriptional phenotype is likely acquired as T cells traffic to the CNS as *Ets1*-KO $CD4^+$ T cells isolated from the spleen showed no such transcriptional alterations and *Ets1*-KO $CD4^+$ T cells before transfer did not display changes in the expression of activation molecules or the cytokines IFN- γ and IL-17A (Extended Data Fig. 7). The findings that ETS1 appears to restrict both the trafficking of T cells to the CNS and their proinflammatory and possibly cytotoxic actions in the target tissue makes this transcriptional regulator an interesting target for therapeutic applications.

Essential regulators are associated with the CNS migration propensity of T cells in multiple sclerosis

To further assess the translational relevance of our findings, we performed single-cell transcriptomic analysis of 70,594 antigen-experienced $CD4^+$ T cells isolated from the blood and 16,575 such cells isolated from the cerebrospinal fluid (CSF) of four untreated participants with MS and four control participants who had been diagnosed with idiopathic intracranial hypertension (IIH; Fig. 7a, for details, see Methods). Bioinformatic analysis revealed 12 distinct $CD4^+$ helper T cell clusters (here termed T1 to T12) that differed in their level of activation, cytotoxicity and exhaustion, as well as a cluster of regulatory T (T_{reg}) cells defined by FOXP3 expression (Fig. 7b,c and Extended Data Fig. 8). All T cell clusters were present in participants with MS and controls and all except for T12 were present in both blood and CSF (Fig. 7d and Methods). To identify those T cell clusters in the blood of participants with MS that are most likely to migrate to the CNS, we used their T cell antigen receptor (TCR) sequences as tags to determine the proportion of T cell clones in each cluster that were also found in the CSF compartment of the same participant (Fig. 7e). In line with the view that these ‘overlapping’ T cell clones have a higher propensity for CNS migration, a differential gene expression analysis showed that overlapping cells upregulate pathways associated with cell adhesion and cell

migration (Extended Data Fig. 9). We then investigated whether this ‘CNS migration propensity’ of a $CD4^+$ T cell cluster correlates with the expression pattern of the key components of the functional modules of CNS migration we identified in the EAE model and found that it did. HSP90B1, GNAI2 and SIPR1 expression levels in $CD4^+$ T cell clusters from participants with MS were significantly correlated with their likelihood of migration into the CNS, while the expression level of ETS1, which limits CNS migration of T cells in rats, showed a trend toward a negative correlation with migration propensity (Fig. 7f). The expression of most of these regulators did not shift markedly after CNS entry as their expression (except for ITGA4, CXCR3 and ETS1) was comparable in T cell clones that were present both in the blood and CNS compartment (Extended Data Fig. 10). Finally, we asked whether the expression of the key components of the functional modules of CNS migration differed between T cells isolated from the blood of participants with MS and controls. We found that FERMT3, HSP90B1, GNAI2 and GRK2 were similarly expressed in $CD4^+$ T cell clusters from participants with MS and controls, while the expression levels of ITGA4, CXCR3, SIPR1 and ETS1 were significantly higher in some of the T cell clusters from participants with MS (Fig. 7g). Notably, the differences in expression level of these key regulatory genes between cells from participants with MS and controls were greater in clusters with a higher migration propensity, again except for the negative regulator ETS1 (Fig. 7h). Taken together, our single-cell transcriptomic analysis of human helper T cells demonstrates that the essential regulators of T cell migration we identified in the rodent MS model are present in a sizable fraction of $CD4^+$ T cells in the blood of participants with MS where their expression correlates with the capacity to enter the CNS.

Discussion

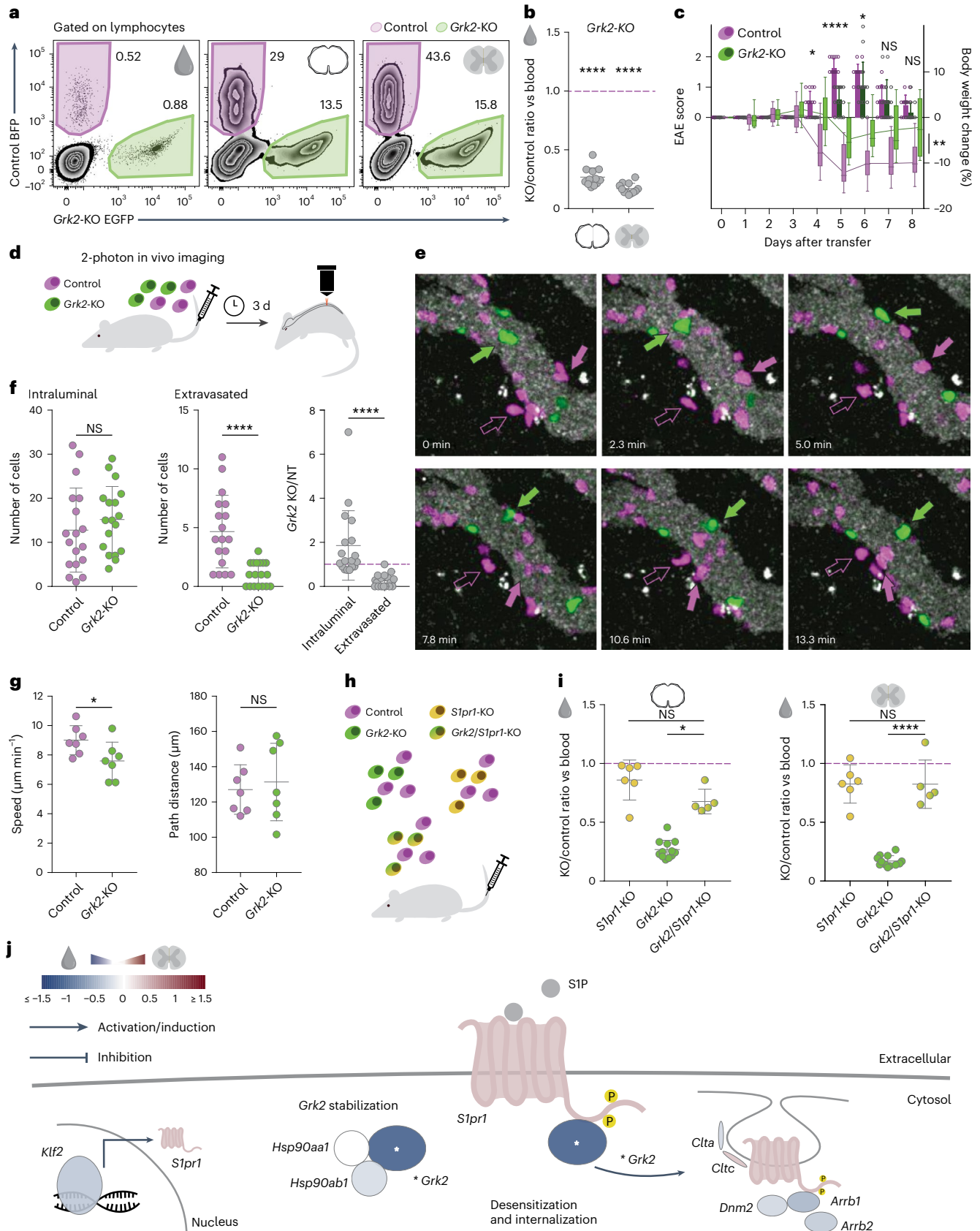
Here we present the results of a genome-wide CRISPR screen aiming to identify the key molecules that regulate the critical initial step in the formation of the MS lesion: the infiltration of autoreactive $CD4^+$ T cells from the blood to the CNS. We reveal the molecules that act as essential brakes and facilitators of the CNS transmigration of T cells, outline the modules that mediate their functional impact and show that their key molecular interactions are conserved across species. Our data also form the foundation for future studies that extend these findings, for example, by looking at the role of paracrine or systemic signals emitted by the cells in question (for example, cytokines, chemokines or matrix metalloproteases released by the autoreactive T cells), or that search for functionally important but molecularly redundant regulatory mechanisms, neither of which can be assessed using a CRISPR screen. Further limitations of the CRISPR screen approach include that molecules can be missed if they only regulate the trafficking of a smaller subset of the studied cell population. Finally, false positive results may arise if a gene regulates a functional property such as T cell activation that is likely required for subsequent CNS migration. We believe this

Fig. 4 | Functional validation of the egress module. **a**, Representative flow cytometry plots of T cells from blood, meninges and parenchyma after a co-transfer experiment. **b**, Migratory phenotype of *Grk2*-KO cells compared to control, shown as the ratio of KO/control in meninges (left) or parenchyma (right) normalized to the KO/control ratio in blood. $n = 12$ rats. **c**, EAE score (bars) and weight changes (line) of control and *Grk2*-KO injected animals; $n = 15$ rats per group. **d**, Experimental design for intravital two-photon imaging. **e**, Time-lapse images tracking cells along the meningeal vasculature. Lilac indicates control cells, and green indicates *Grk2*-KO cells; filled arrows indicate cells inside the blood vessel lumen, and empty arrows indicate extravasated cells. **f**, Distribution of cells in the leptomeninges vasculature. Left, intraluminal cell count; middle, extravasated cell count; right, ratio of KO/control cells derived from data in the previous two plots. $n = 3$ animals, 5–7 images per animal, for a total $n = 18$ images. **g**, Analysis of speed (left) and path distance (right) of cells crawling in the blood vessels. Data summarized per movie, $n = 3$ animals, 2–3 movies per animal, 15–76 cells per condition per movie, for a total $n = 7$ movies. **h**, Experimental design.

i, Migratory phenotype of KO T_{MBP} cells compared to control T_{MBP} cells, shown as the ratio of KO to control in meninges (left) or parenchyma (right) divided by the KO/control ratio in blood. $n = 6$ rats for *S1pr1*-KO; $n = 12$ rats for *Grk2*-KO same data as in **b**; $n = 5$ rats for *Grk2/S1pr1*-KO. **j**, Schematic of the egress module with genes color coded based on the parenchyma versus blood comparison. Asterisks indicate significance across at least three pairwise tissue comparisons (Methods). **b**, One-sample *t*-test against hypothetical mean = 1; **c**, bars and dots, EAE score; box-and-whiskers plot and line, body weight change; repeated-measures two-way ANOVA (days 3–8 for disease score ($F = 13.82$, $P = 0.0009$) and days 0–8 for weight changes ($F = 12.69$, $P = 0.0013$)) and Sidak’s multiple-comparison test only for EAE score; **f, g**, Paired parametric *t*-test or Wilcoxon matched-pairs signed-rank test; **i**, Kruskal–Wallis test (Kruskal–Wallis = 17.01, $P = 0.0002$) with Dunn’s multiple-comparison test for meninges, and one-way ANOVA ($F = 75.6$, $P < 0.0001$) with Turkey’s multiple-comparison test for parenchyma. Figures show the mean \pm s.d. NS, $P > 0.05$, * $P < 0.05$, ** $P < 0.01$, *** $P < 0.001$, **** $P < 0.0001$.

is unlikely to be the case for the essential regulators we identify here because a comparison between the activated and expanded T cells at the end of the culture period with the plasmid library showed a depletion of genes associated with T cell activation and proliferation but did

not show a marked regulation of the essential mediators of migration (Extended Data Fig. 1). Despite its limitations, the CRISPR-based screening of MS models that we introduce here represents a highly versatile approach that can be easily adapted to interrogate the subsequent



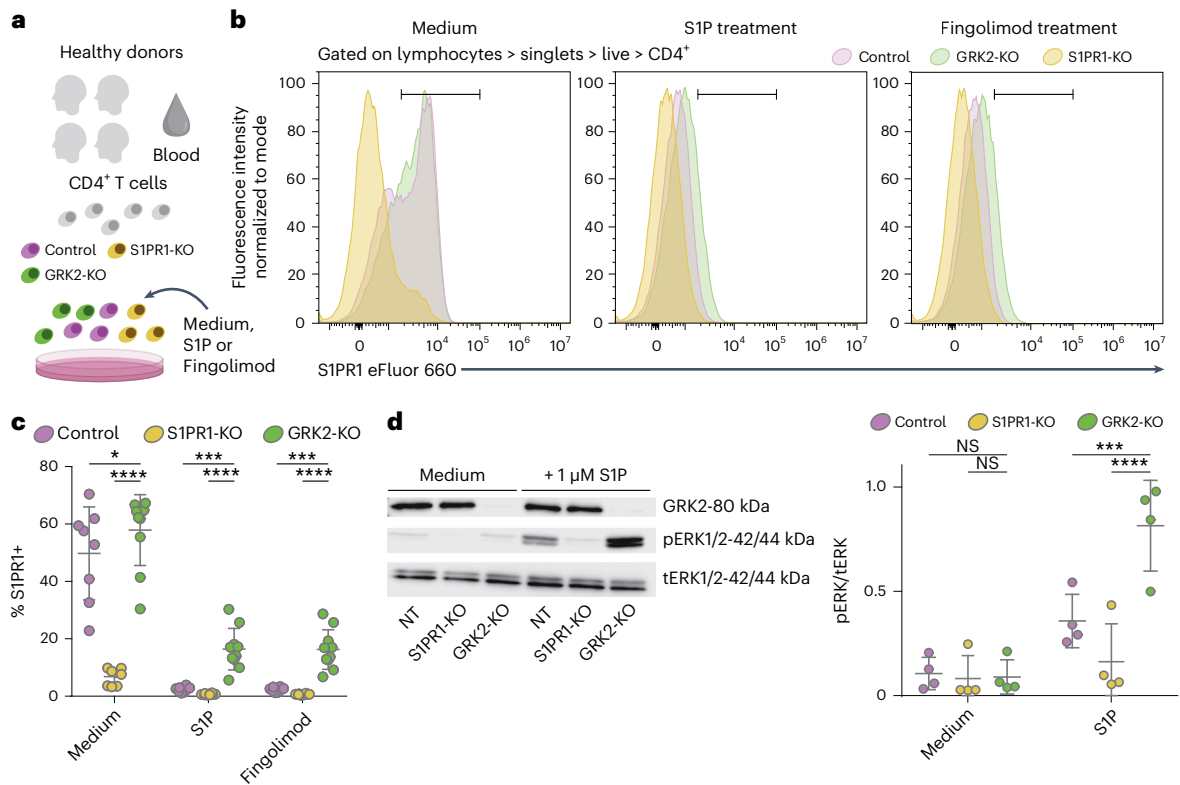


Fig. 5 | GRK2 mediates S1PR1 internalization in human T cells. **a**, Scheme of the experimental design. CD4⁺ T cells were collected from the buffy coats of healthy donors and CRISPR KO cells were generated in vitro. Cells were treated with control medium, S1P or fingolimod, and S1PR1 internalization was measured by fluorescence-activated cell sorting (FACS) surface staining. **b**, Representative flow cytometry plots of control and KO T cells for medium, S1P and fingolimod treatment conditions. **c**, Quantification of the percentage of S1PR1 surface expression after treatment. $n = 1-3$ independent internalization assays from four donors for all groups, for a total of $n = 8$ control and S1PR1-KO, $n = 10$ GRK2-KO

S1PR1 internalization assays. **d**, Representative western blot image (left) and quantification (right) of MAPK (ERK1/ERK2) phosphorylation following S1PR1 stimulation with the endogenous ligand S1P. Phospho-ERK1/ERK2 values are shown normalized to total ERK1/ERK2. $n = 4$ donors. Phospho-ERK1/ERK2 and total ERK1/ERK2 blots were run in parallel, GRK2 was stained in the phospho-ERK1/ERK2 blot. **c, d**, Two-way ANOVA (**c**, $F = 83.26$, $P < 0.0001$; **d**, $F = 11.13$, $P = 0.0007$) with multiple comparisons with the two-stage linear step-up procedure of Benjamini, Krieger and Yekutieli. Figures show the mean \pm s.d. NS, $P > 0.05$, * $P < 0.05$, ** $P < 0.01$, *** $P < 0.001$, **** $P < 0.0001$.

steps of T cell-mediated CNS pathology or could be leveraged to resolve the migration of other immune cells with critical contributions to MS pathology such as CD8⁺ T cells, B cells or monocytes.

What did we learn from this unbiased and comprehensive characterization of the essential molecular signals governing autoreactive T cell entry to the CNS? First, that remarkably few molecules are essential for T cell migration into the CNS, and that the majority of the most potent mediators naturally cluster in three functional modules: one centered around the adhesion molecule $\alpha 4$ -integrin, another around the chemokine receptor CXCR3 and the final one involving the S1PR1-GRK2 axis. While some of these molecules have been implicated in T cell migration in general, or even in MS, before,

this unbiased analysis reveals all nonredundant targets among their transcriptional regulators, chaperones and binding partners as well as their intracellular signaling streams. Alongside, many previously suspected candidate regulators did not appear as ‘essential’ in our screen. These included the CCR5, CCR6 and CCR7 chemokine receptors^{7,39,40}, the adhesion molecules P-selectin⁴¹, Ninjurin-1 (refs. 5,42), MCAM⁴³, DICAM⁴⁴, the ALCAM ligand CD6 (refs. 45,46) and LFA-1 (ref. 47). This raises interesting questions around whether these mediators are functionally redundant, or whether they are only required for a subpopulation of CD4⁺ T cells, as for LFA-1, MCAM and DICAM, which are primarily important for the migration of the T_H17 subset of helper T cells^{43,44,48}.

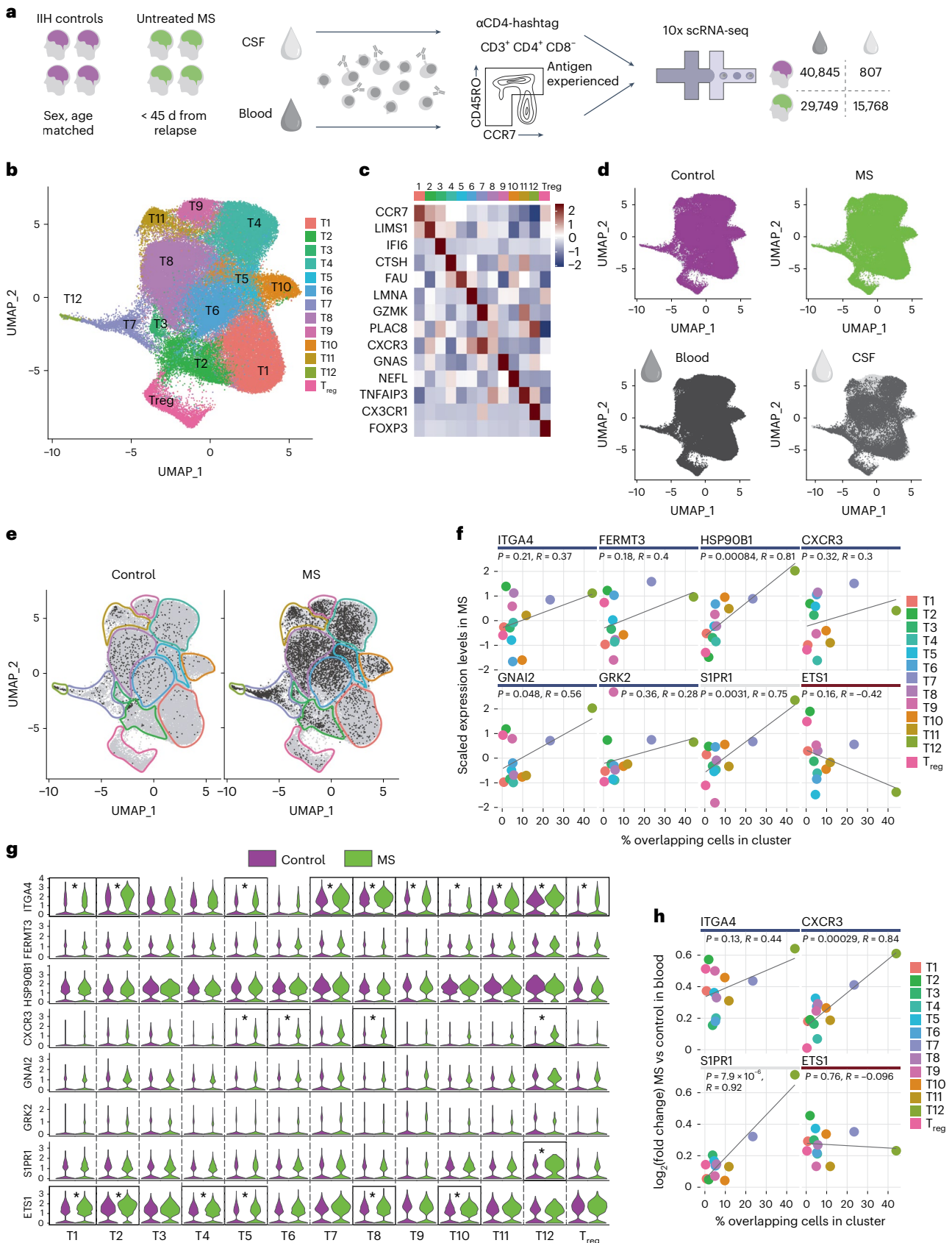
Fig. 6 | ETS1 inhibits CD4⁺ T cell migration to the CNS. **a**, Representative flow cytometry plots of T cells from blood, meninges and parenchyma after a co-transfer experiment with control and *Ets1*-KO T_{MBP} cells. **b**, Migratory phenotype of *Ets1*-KO cells compared to control, shown as the ratio of KO/control in meninges (left) or parenchyma (right) normalized to the KO/control ratio in blood. $n = 12$ rats. **c**, Experimental design of the bulk RNA sequencing (RNA-seq) of *Ets1*-KO and control cells from the parenchyma of co-transferred animals. **d**, Volcano plot of the RNA-seq results of *Ets1*-KO cells compared to control T_{MBP} cells. Lines at P value = 0.05 and \log_2 (fold change) = ± 3 standard deviations of the \log_2 (fold change) of the sample. Green indicates significantly differentially expressed genes, with black circles around those belonging to pathways in **e**; blue indicates essential genes ‘facilitating’ CNS migration in T_{MBP} cells (‘CRISPR

impaired migration’); red indicates essential genes ‘braking’ CNS migration (‘CRISPR enhanced migration’) in T_{MBP} cells derived from Fig. 1d,f. **e**, Pathway analysis of the top downregulated and top upregulated pathways in the *Ets1*-KO compared to control T_{MBP} cells. **f**, Significant (adjusted $P < 0.05$ and absolute \log_2 (fold change) > 3 standard deviations of the sample) genes belonging to the pathways in **e**. **g**, Experimental design of the bulk RNA-seq of *Ets1*-KO and control human CD4⁺ T cells. **h**, Correlation between *Ets1*-KO versus control \log_2 (fold change) in rat and *ETS1*-KO versus control \log_2 (fold change) in human. Green indicates genes regulated in both species (P value < 0.05 in at least one species and absolute \log_2 (fold change) > 2 times the standard deviation of the sample in both). **i**, One-sample t -test against hypothetical mean = 1. Figures show the mean \pm s.d. NS, $P > 0.05$, * $P < 0.05$, ** $P < 0.01$, *** $P < 0.001$, **** $P < 0.0001$.

A second important finding of our screen is the presence of endogenous ‘brakes’ of T cell migration, such as the transcription factor ETS1, which appears to limit the responsiveness of T cells to a range of immunological signals. Notably, ETS1 also appears to restrict the expression of a number of cytotoxic mediators making the induction

of this transcriptional regulator an attractive strategy in autoimmune conditions. Furthermore, inhibition of ETS1 might be of therapeutic interest in the context of brain cancer or neurodegenerative diseases in which insufficient immune responses in the CNS can contribute to pathology^{49,50}.





Importantly, we showed that the essential modules we identified in the rat EAE model have high likelihood of relevance in participants with MS. Two of the major clinical strategies that limit CNS infiltration of T cells in people with MS, blocking α 4-integrin and interfering

with the S1PR1 receptor, also emerge as central functional hubs in our genome-wide screen. While established S1PR1 modulators induce receptor internalization, we show here that interfering with receptor desensitization via GRK2 is a distinct regulatory mechanism that is

Fig. 7 | Expression of essential regulators of migration in T cells from participants with multiple sclerosis. **a**, Single-cell RNA-seq (scRNA-seq) experimental design. Sorted CD4⁺ T cells from the blood and whole CSF of untreated participants with MS, or sex-matched and age-matched controls, were collected and analyzed. **b**, CD4⁺ T cell clusters. **c**, Cluster-defining genes. **d**, Distribution of control or MS samples, and of blood or CSF samples, across the clusters. **e**, Overlapping cells in control and MS, across clusters, defined as cells whose TCR was found in blood and CSF of the same participant. **f**, Correlations between the percentage of overlapping cells per cluster and the relative gene expression level of essential regulators in this cluster in MS blood. **g**, Violin plots

of the candidate genes expression level across clusters, comparing control (lilac) and MS (green) cell samples from blood. Asterisks indicate significance; adjusted *P* value < 0.05 and absolute log₂(fold change) > 3 times the standard deviation of the sample. **h**, Correlations between the percentage of overlapping cells per cluster and the log₂(fold change) of gene expression in this cluster between MS and control blood, for those essential regulators that show differences in expression levels between MS compared to control blood as in **g**. **f, h**, *R* value and *P* values correspond to a Pearson correlation. **g**, Asterisks correspond to adjusted *P* values < 0.05 comparing MS to control blood.

active in human T cells and has an even more potent effect on CNS migration, at least in our rodent MS model. Interestingly, a previous study reported reduced GRK2 protein levels in peripheral blood mononuclear cells (PBMCs) isolated from people with relapsing–remitting and secondary progressive MS suggesting an altered regulation of S1PR1 internalization³¹. We further show that the expression pattern of the essential regulators we identified in the EAE model reflects the propensity of defined T cell clusters from individuals with MS to reach the CNS. Alongside, the expression of several of these regulators, most prominently of α4-integrin and CXCR3, is specifically higher in CNS migration-prone T cell clusters in individuals with MS compared to controls. These data extend the results from previous population-based analyses of T cells in people with MS^{51,52} and provide a molecular explanation for enhanced T cell entry to the CNS in MS. Taken together, our study thus helps to define the essential molecules and modules that govern CD4⁺ T cell trafficking to the CNS and demonstrates their regulated expression in individuals with MS.

Online content

Any methods, additional references, Nature Portfolio reporting summaries, source data, extended data, supplementary information, acknowledgements, peer review information; details of author contributions and competing interests; and statements of data and code availability are available at <https://doi.org/10.1038/s41593-023-01432-2>.

References

- Steinman, L. Immunology of relapse and remission in multiple sclerosis. *Annu. Rev. Immunol.* **32**, 257–281 (2014).
- Reich, D. S., Lucchinetti, C. F. & Calabresi, P. A. Multiple sclerosis. *N. Engl. J. Med.* **378**, 169–180 (2018).
- Attfield, K. E., Jensen, L. T., Kaufmann, M., Friese, M. A. & Fugger, L. The immunology of multiple sclerosis. *Nat. Rev. Immunol.* **22**, 734–750 (2022).
- Ben-Nun, A. & Cohen, I. R. Vaccination against autoimmune encephalomyelitis (EAE): attenuated autoimmune T lymphocytes confer resistance to induction of active EAE but not to EAE mediated by the intact T lymphocyte line. *Eur. J. Immunol.* **11**, 949–952 (1981).
- Odoardi, F. et al. T cells become licensed in the lung to enter the central nervous system. *Nature* **488**, 675–679 (2012).
- Bartholomäus, I. et al. Effector T cell interactions with meningeal vascular structures in nascent autoimmune CNS lesions. *Nature* **462**, 94–98 (2009).
- Schläger, C. et al. Effector T-cell trafficking between the leptomeninges and the cerebrospinal fluid. *Nature* **530**, 349–353 (2016).
- Yednock, T. A. et al. Prevention of experimental autoimmune encephalomyelitis by antibodies against alpha 4 beta 1 integrin. *Nature* **356**, 63–66 (1992).
- Sawcer, S. et al. Genetic risk and a primary role for cell-mediated immune mechanisms in multiple sclerosis. *Nature* **476**, 214–219 (2011).
- Ingelfinger, F. et al. Twin study reveals non-heritable immune perturbations in multiple sclerosis. *Nature* **603**, 152–158 (2022).
- Kaufmann, M. et al. Identifying CNS-colonizing T cells as potential therapeutic targets to prevent progression of multiple sclerosis. *Med.* **2**, 296–312 (2021).
- Tintore, M., Vidal-Jordana, A. & Sastre-Garriga, J. Treatment of multiple sclerosis—success from bench to bedside. *Nat. Rev. Neurol.* **15**, 53–58 (2019).
- Wang, T. et al. Gene essentiality profiling reveals gene networks and synthetic lethal interactions with oncogenic Ras. *Cell* **168**, 890–903 (2017).
- Weber, J., Braun, C. J., Saur, D. & Rad, R. In vivo functional screening for systems-level integrative cancer genomics. *Nat. Rev. Cancer* **20**, 573–593 (2020).
- Shifrut, E. et al. Genome-wide CRISPR screens in primary human T cells reveal key regulators of immune function. *Cell* **175**, 1958–1971 (2018).
- Chen, Z. et al. In vivo CD8⁺ T cell CRISPR screening reveals control by Flt1 in infection and cancer. *Cell* **184**, 1262–1280 (2021).
- Del Galy, A. S. et al. In vivo genome-wide CRISPR screens identify SOCS1 as intrinsic checkpoint of CD4⁺ T_H1 cell response. *Sci. Immunol.* **6**, eabe8219 (2021).
- Kawakami, N. et al. The activation status of neuroantigen-specific T cells in the target organ determines the clinical outcome of autoimmune encephalomyelitis. *J. Exp. Med.* **199**, 185–197 (2004).
- Bock, C. et al. High-content CRISPR screening. *Nat. Rev. Methods Primers* **2**, 9 (2022).
- Li, W. et al. MAGeCK enables robust identification of essential genes from genome-scale CRISPR/Cas9 knockout screens. *Genome Biol.* **15**, 554 (2014).
- Zhao, L. et al. CFBF-MYH11 hinders early T-cell development and induces massive cell death in the thymus. *Blood* **109**, 3432–3440 (2007).
- Koch, M. A. et al. The transcription factor T-bet controls regulatory T cell homeostasis and function during type 1 inflammation. *Nat. Immunol.* **10**, 595–602 (2009).
- Newton, R. H. et al. Maintenance of CD4 T cell fitness through regulation of Foxo1. *Nat. Immunol.* **19**, 838–848 (2018).
- Garg, G. et al. Blimp1 prevents methylation of Foxp3 and loss of regulatory T cell identity at sites of inflammation. *Cell Rep.* **26**, 1854–1868 (2019).
- Śledzińska, A. et al. Regulatory T cells restrain interleukin-2- and Blimp-1-dependent acquisition of cytotoxic function by CD4⁺ T Cells. *Immunity* **52**, 151–166 (2020).
- Zhang, Q. et al. Ska3 phosphorylated by Cdk1 binds Ndc80 and recruits Ska to kinetochores to promote mitotic progression. *Curr. Biol.* **27**, 1477–1484 (2017).
- Liu, B. & Li, Z. Endoplasmic reticulum HSP90b1 (gp96, grp94) optimizes B-cell function via chaperoning integrin and TLR but not immunoglobulin. *Blood* **112**, 1223–1230 (2008).
- Moretti, F. A. et al. Kindlin-3 regulates integrin activation and adhesion reinforcement of effector T cells. *Proc. Natl Acad. Sci. USA* **110**, 17005–17010 (2013).
- DeNucci, C. C., Pagán, A. J., Mitchell, J. S. & Shimizu, Y. Control of alpha4beta7 integrin expression and CD4 T cell homing by the beta1 integrin subunit. *J. Immunol.* **184**, 2458–2467 (2010).

30. Thompson, B. D. et al. Inhibition of G α i2 activation by G α i3 in CXCR3-mediated signaling. *J. Biol. Chem.* **282**, 9547–9555 (2007).
31. Vroon, A., Lombardi, M. S., Kavelaars, A. & Heijnen, C. J. Changes in the G-protein-coupled receptor desensitization machinery during relapsing-progressive experimental allergic encephalomyelitis. *J. Neuroimmunol.* **137**, 79–86 (2003).
32. Penela, P., Ribas, C., Sánchez-Madrid, F. & Mayor, F. G protein-coupled receptor kinase 2 (GRK2) as a multifunctional signaling hub. *Cell. Mol. Life Sci.* **76**, 4423–4446 (2019).
33. Arnon, T. I. et al. GRK2-dependent S1PR1 desensitization is required for lymphocytes to overcome their attraction to blood. *Science* **333**, 1898–1903 (2011).
34. Lee, M. J., Evans, M. & Hla, T. The inducible G-protein-coupled receptor edg-1 signals via the Gi/mitogen-activated protein kinase pathway. *J. Biol. Chem.* **271**, 11272–11279 (1996).
35. McGinley, M. P. & Cohen, J. A. Sphingosine 1-phosphate receptor modulators in multiple sclerosis and other conditions. *Lancet* **398**, 1184–1194 (2021).
36. Zook, E. C. et al. The ETS1 transcription factor is required for the development and cytokine-induced expansion of ILC2. *J. Exp. Med.* **213**, 687–696 (2016).
37. Kim, C. J. et al. The transcription factor Ets1 suppresses T follicular helper type 2 cell differentiation to halt the onset of systemic lupus erythematosus. *Immunity* **49**, 1034–1048 (2018).
38. Lee, C. G. et al. Ets1 suppresses atopic dermatitis by suppressing pathogenic T cell responses. *JCI insight* **4**, e124202 (2019).
39. Yamazaki, T. et al. CCR6 regulates the migration of inflammatory and regulatory T cells. *J. Immunol.* **181**, 8391–8401 (2008).
40. Belikan, P. et al. CCR7 on CD4⁺ T cells plays a crucial role in the induction of experimental autoimmune encephalomyelitis. *J. Immunol.* **200**, 2554–2562 (2018).
41. Sathiyandan, K., Coisne, C., Enzmann, G., Deutsch, U. & Engelhardt, B. PSGL-1 and E/P-selectins are essential for T-cell rolling in inflamed CNS microvessels but dispensable for initiation of EAE. *Eur. J. Immunol.* **44**, 2287–2294 (2014).
42. Ifergan, I. et al. Role of Ninjurin-1 in the migration of myeloid cells to central nervous system inflammatory lesions. *Ann. Neurol.* **70**, 751–763 (2011).
43. Larochelle, C. et al. Melanoma cell adhesion molecule identifies encephalitogenic T lymphocytes and promotes their recruitment to the central nervous system. *Brain* **135**, 2906–2924 (2012).
44. Charabati, M. et al. DICAM promotes T_H17 lymphocyte trafficking across the blood–brain barrier during autoimmune neuroinflammation. *Sci. Transl. Med.* **14**, eabj0473 (2022).
45. Cayrol, R. et al. Activated leukocyte cell adhesion molecule promotes leukocyte trafficking into the central nervous system. *Nat. Immunol.* **9**, 137–145 (2008).
46. Freitas, R. F. et al. Modulation of CD4 T cell function via CD6-targeting. *EBioMedicine* **47**, 427–435 (2019).
47. Walling, B. L. & Kim, M. LFA-1 in T cell migration and differentiation. *Front. Immunol.* **9**, 952 (2018).
48. Rothhammer, V. et al. T_H17 lymphocytes traffic to the central nervous system independently of α 4 integrin expression during EAE. *J. Exp. Med.* **208**, 2465–2476 (2011).
49. Daubon, T., Hemadou, A., Romero Garmendia, I. & Saleh, M. Glioblastoma immune landscape and the potential of new immunotherapies. *Front. Immunol.* **11**, 585616 (2020).
50. Dujardin, P., Vandenbroucke, R. E. & Van Hoecke, L. Fighting fire with fire: the immune system might be key in our fight against Alzheimer’s disease. *Drug Discov. Today* **27**, 1261–1283 (2022).
51. Jensen, J., Krakauer, M. & Sellebjerg, F. Cytokines and adhesion molecules in multiple sclerosis patients treated with interferon-beta1b. *Cytokine* **29**, 24–30 (2005).
52. Balashov, K. E., Rottman, J. B., Weiner, H. L. & Hancock, W. W. CCR5⁺ and CXCR3⁺ T cells are increased in multiple sclerosis and their ligands MIP-1 α and IP-10 are expressed in demyelinating brain lesions. *Proc. Natl Acad. Sci. USA* **96**, 6873–6878 (1999).

Publisher’s note Springer Nature remains neutral with regard to jurisdictional claims in published maps and institutional affiliations.

Open Access This article is licensed under a Creative Commons Attribution 4.0 International License, which permits use, sharing, adaptation, distribution and reproduction in any medium or format, as long as you give appropriate credit to the original author(s) and the source, provide a link to the Creative Commons license, and indicate if changes were made. The images or other third party material in this article are included in the article’s Creative Commons license, unless indicated otherwise in a credit line to the material. If material is not included in the article’s Creative Commons license and your intended use is not permitted by statutory regulation or exceeds the permitted use, you will need to obtain permission directly from the copyright holder. To view a copy of this license, visit <http://creativecommons.org/licenses/by/4.0/>.

© The Author(s) 2023

Methods

Contact for reagent and resource sharing

Further information and requests for resources and reagents should be directed to and will be fulfilled by N.K. Plasmids generated in this study are available upon reasonable request.

Experimental model and participant details

Plasmids. All primer sequences are listed in Supplementary Table 3.

The pMSCV-Cas9-EGFP vector was constructed as follows. First, a Cas9-p2a-EGFP construct was PCR amplified from the Lenti-Cas9-EGFP plasmid obtained from Addgene (63592). Then, the PCR product was assembled into an EcoRI + XhoI digested pMSCV-neo (Takara Clontech) vector by using Gibson Assembly Master Mix (NEB). The gRNA expression vector MSCV-pU6-(BbsI)-CcdB-(BbsI)-Pgk-Puro-T2A-BFP was obtained from Addgene (86457). The MSCV-v2-U6-(BbsI)-Pgk-Puro-T2A-GFP (with v2 improved scaffold) vector was generated as follows: first, the pU6-Pgk-Puro-T2A construct was PCR amplified from pKLV2-U6gRNAs(BbsI)-PGKpuro2ABFP-W (Addgene, 67974), and the EGFP construct was PCR amplified from pMSCV-Cas9-EGFP; then, the PCR product was assembled into the Sall + XhoI digested pMSCV-neo vector using the Gibson Assembly Master Mix. The pMSCV-v2-U6-(BbsI)-Pgk-Puro-T2A-BFP (with v2 improved scaffold) vector was generated as follows: the pU6-Pgk-Puro-T2A-BFP construct was PCR amplified with overhangs for Sall + XhoI from pKLV2-U6gRNAs(BbsI)-PGKpuro2ABFP-W, then the PCR product was digested and ligated into Sall + XhoI digested pMSCV-neo vector with Quick Ligase (NEB).

Animals. Lewis rats were purchased from Charles River (LEW/Crl) or Janvier (LEW/OrlRj) and bred in the Core Facility Animal Models of the Biomedical Center, LMU. All animal experiments and their care were carried out in accordance with the regulations of the applicable animal welfare acts and protocols were approved by the responsible regulatory authority (Regierung von Oberbayern). All animals had free access to food and water. Animals were kept at room temperature 22 ± 2 °C, humidity $55 \pm 10\%$ with a light–dark cycle, 12 h/12 h (6:30–18:30). Male and female Lewis rats between 5 and 20 weeks old were used for the experiments. The animals were allocated randomly for experimental groups.

Generation of Cas9-expressing T_{MBP} cells. Cultures of T_{MBP} cells were established as previously described⁵³. Briefly, a Lewis rat was immunized in the hind-limb flanks with 100 µg guinea pig MBP (purified in-house) emulsified with complete Freund's adjuvant (Difco). Draining lymph nodes were collected 10 d after immunization and a single-cell suspension was prepared by passing through a metal strainer. The cells were then restimulated *ex vivo* with 10 µg ml⁻¹ MBP either together with retrovirus producing GP + E86 (American Type Culture Collection (ATCC) packaging cells stably transfected with pMSCV-Cas9-EGFP, or without packaging cells, in complete DMEM supplemented with 1% rat serum. Two days later, TCGF (complete DMEM supplemented with 10% horse serum and 2% of phorbol myristate acetate (PMA)-stimulated EL4IL2 cell culture supernatant) was added to expand the number of T cells. After 4 d of expansion culture, the T cells were restimulated for 2 d with 50-Gy irradiated thymocytes in complete DMEM supplemented with 1% rat serum and 10 µg ml⁻¹ MBP, which was followed by another round of expansion in TCGF for 4 d. This cycle of restimulation and expansion was repeated before some experiments. In addition, successfully transduced T cells were enriched by adding 400 µg ml⁻¹ neomycin for 8 d from 4 d after the first stimulation and sorting for GFP⁺ cells with a BD FACSAria IIIu operated with FACSDiva. The antigen specificity of the cultured T cells was confirmed by a proliferation assay, as described previously⁴⁸. Cells were frozen in a 10% dimethyl sulfoxide/90% FBS mixture at -80 °C, or stored in liquid nitrogen for long-term storage.

Study participants. CSF sampling was performed to confirm the diagnosis of relapsing–remitting MS according to the revised McDonald criteria for all (four) participants included in the study, who had encountered an MS relapse in the 45 d before lumbar puncture and had not received any disease-modifying treatments (one participant was treated with high-dose steroids 24 d before sampling). CSF and blood samples from four sex-matched and age-matched individuals diagnosed with IHH were included as the control group. Participant samples were collected at the Institute of Clinical Neuroimmunology at the LMU Klinikum Munich, Germany. Recruitment of participants took place from August 2020 to January 2021. Collection of blood and CSF was approved by the local ethics committees of the LMU, Munich (ethical vote no. 163-16). Written informed consent was obtained from all participants according to the Declaration of Helsinki.

PBMCs of four healthy donors used for CRISPR gene editing were derived from leukoreduction system chambers provided by the Department of Transfusion Medicine at the LMU Klinikum Munich, Germany (ethical vote LMU no. 18-821).

Method details

Genome-wide rat guide RNA library construction. A list of sgRNAs targeting genes and miRNAs in the rat genome was kindly provided by the Functional Genomics Consortium of The Broad Institute, Massachusetts, USA. All sgRNA sequences that were selected, and the library cloning primers, as well as protocols, are listed in Supplementary Table 3.

For the genome-wide library, in nearly all cases four sgRNA per gene or miRNA were selected; in some cases, for example, for miRNAs only fewer unique sgRNAs were available. A total of 87,690 oligonucleotides were purchased from Twist Bioscience, each as a 79-mer with a sequence of 5'-GCAGATGGCTCTTTGTCCTAGACATC-GAAGACAACACCGN₂₀GTTTTAGTCTTCTCGTCGCC-3', N₂₀ indicating the sgRNA sequence. Library cloning was performed as previously described⁵⁴ with minor modifications to the primer sequences and protocol (Supplementary Table 3). Briefly, oligonucleotide pools were dissolved in TE buffer at a 10 ng µl⁻¹ stock concentration, then the single-stranded oligonucleotides (1 ng) were PCR amplified for 10 cycles with Q5 High Fidelity DNA Polymerase (NEB) using Oligo_Amp_F and Oligo_Amp_R primers to generate double-stranded DNAs. A total of 24 reactions were pooled. The PCR products were purified with the Nucleotide Removal Kit (Qiagen). Amplified double-stranded DNAs were digested with FastDigest BpiI (BbsI: Thermo Fisher) for 2 h at 37 °C in a total of 20 reactions, and then purified with the Nucleotide Removal Kit. Ligation was performed with a T4 DNA Ligase (NEB) using a 3-ng insert and 40 ng BpiI-digested MSCV-pU6-(BbsI)-CcdB-(BbsI)-Pgk-Puro-T2A-BFP for 16 h at 16 °C per reaction in a total of 30 reactions. The ligated product was cleaned with a PCR Purification Kit (Qiagen) and the concentration was measured with Qubit 4 (Thermo Fisher). Next, 10 ng of the ligated product was transformed into 50 µl of NEB Stable Competent cells in a total of 45 reactions and incubated at 30 °C overnight. A library representation above 100× was confirmed by plating transformed competent cells in serial dilutions. The plasmid DNA was prepared with an Endofree Plasmid Maxi Kit (Qiagen). For the validation library, six sgRNAs were used per gene whenever possible. An oligonucleotide pool containing 12,000 oligonucleotides was purchased from Twist Bioscience and plasmid DNA was prepared similarly to the genome-wide library.

Gene editing of T_{MBP} cells. For viral transduction of CRISPR sgRNAs, 1.2×10^6 HEK293T cells (ATCC) in complete DMEM with 10% FBS were plated into a 10-cm diameter culture dish 18–24 h before transfection. For the transfection, 6 µg pMSCV retroviral plasmid and 3.5 µg pCL-Eco packaging vector were preincubated in 500 µl of complete DMEM at room temperature for 15 min before mixing with 500 µl of 80 µg ml⁻¹ PEI max (Polysciences) in complete DMEM. After 20 min, the solution was added dropwise to HEK293T cells. The cells were cultured in 5%

CO₂ at 37 °C for 24 h and the medium was replaced with 8 ml complete DMEM + 10% FBS for detoxification. The cells were cultured in 10% CO₂ at 37 °C, and retrovirus-containing supernatant was collected at 48 h and 72 h after transfection. The supernatant was then passed through a 0.45-µm filter to remove debris and virus was concentrated using Amicon Ultra-15 Centrifugal Filter Units (Sigma). For this, 14 ml supernatant was centrifuged at 4,000g for 20 min at room temperature. The concentrated virus was used immediately for transduction of rat T cells.

For transduction, freshly restimulated T cells were resuspended in DMEM with 25 mM HEPES and then enriched by Nycoprep gradient centrifugation at 800g for 10 min at room temperature. The T cells were resuspended at concentration of 4 × 10⁶ per ml in TCGF with 8 µg ml⁻¹ polybrene (Sigma) and this suspension was plated at 500 µl per well in 12-well plates. Finally, concentrated virus solution was added at 50 µl per well and plates were centrifuged at 2,000g, at room temperature for 90 min. TCGF was added at 1 ml per well and T cells were further cultured in 10% CO₂ at 37 °C. T_{MBP} cells were transduced at a maximum MOI of 0.3 to prevent multiple integrations, and enough T cell numbers were kept at all times to ensure a minimum 1,000× coverage in vitro (1,000 T cells having the same sgRNA; 90 × 10⁶ cells for the genome-wide screen and 12 × 10⁶ cells for the validation screen). On the next day, puromycin was added at a final concentration of 0.5 µg ml⁻¹ to select for transduced T cells. After 4 d of culture, the T cells were restimulated as described above for 2 d, before injection into recipient animals. For T cell transfer into animals, cell numbers injected were such to maintain a minimum coverage of 1,000× per replicate.

For candidate gene validation, CRISPR sgRNAs were introduced by ribonucleoprotein (RNP) electroporation into previously BFP or EGFP retrovirus transduced T_{MBP} cells. sgRNAs were designed by using the GPP sgRNA designer^{55,56} and synthesized by Integrated DNA Technologies. The Cas9 protein and sgRNA were electroporated into the T cells by using Amaxa 4D-Nucleofector System and P4 Primary Cell 4D-Nucleofector X Kit S (Lonza) according to the manufacturer's instructions. Briefly, to prepare the transfection reagent, 0.75 µl of Alt-R CRISPR-Cas9 trans-activating crRNA (tracrRNA; 200 pmol µl⁻¹) and 0.75 µl of Alt-R CRISPR-Cas9 crRNA (200 pmol µl⁻¹; IDT) were mixed; the solution was then incubated at 95 °C for 5 min, decreasing to 70 °C at the rate of 0.5 °C s⁻¹, at 70 °C for 1 min, then cooled to 22 °C. After adding 7.5 µg Alt-R S.p. HiFi Cas9 Nuclease V3 (IDT), the mixture was incubated at room temperature for 20 min. The master mix was prepared by mixing 18 µl of P4 primary solution, 4 µl of Supplement 1 and 1 µl of electroporation enhancer (stock solution of 100 µM; IDT). After washing with PBS, 2 × 10⁶ T cells were pelleted and resuspended in 21 µl of master mix. This cell suspension was mixed with the transfection reagent and transferred into the Nucleofection cuvette. Electroporation was performed using the pulse code CM137.

Tide assay. All single KO lines used in validation experiments were validated for the KO efficiency before the experiment (Supplementary Table 3). To assess the extent of genetic editing at DNA level for single sgRNAs, cells were lysed by lysis buffer (H₂O with 100 µl ml⁻¹ 1 M Tris, 10 µl ml⁻¹ 0.5 M EDTA, 40 µl ml⁻¹ 3 M NaCl, 5 µl ml⁻¹ Tween 20) supplemented with 5 µl ml⁻¹ Proteinase K for 15 min at 56 °C and 10 min at 95 °C followed by cooling on ice. Then, 350 µl isopropanol was added, incubated for 10 min at room temperature and centrifuged for 10 min at 16,000g at 4 °C. The pellet was washed by addition of 1 ml of 70% ethanol and 5 min centrifugation at 16,000g at 4 °C. After removal of liquid, the pellet was dried for 10 min at 56 °C and resuspended in 50 µl water. PCR amplification of the modified DNA sequence was performed with specific primers for each target using 2× Optima PCR HotStart Polymerase (FastGene). PCR products were run on a 1% agarose gel and amplicons of the expected size were purified using the Wizard SV Gel and PCR Clean-Up System (Promega). For human T cells, genomic DNA was isolated with the DNeasy Blood and Tissue Kit (Qiagen) and the modified DNA region was amplified with Q5 High Fidelity DNA

Polymerase (NEB). The samples were submitted to Sanger Sequencing (Sequencing service, LMU Biozentrum). The INDELS and KO efficiency were assessed by the ICE v2 software tool⁵⁷.

Adoptive transfer experimental autoimmune encephalomyelitis and isolation of T_{MBP} cells. EAE was induced in rats by intravenous adoptive transfer of in vitro activated T_{MBP} cells. Following transfer, body weight and the EAE score of the rats were monitored daily. The EAE score was evaluated as follows: 0, no clinical signs; 0.5, partial tail weakness; 1, tail paralysis; 1.5, gait instability or impaired righting ability; 2, hind-limb paresis; 2.5, hind-limb paresis with dragging of one foot; 3, total hind-limb paralysis. The number of transferred T cells was about 12 × 10⁶ for screening (a minimum of eight animals were pooled for a single genome-wide replicate and a minimum of six animals were pooled per validation screen replicate), a mixture of 3 × 10⁶ control T cells and 3 × 10⁶ KO T cells were transferred for evaluating their migration to the CNS, and 1 × 10⁶ T cells were transferred for the assessment of the clinical course.

For screening and in vivo migration analysis, the animals were euthanized on day three after T cell transfer, when animals showed first clinical symptoms, such as body weight loss and/or a mild clinical score (<1). Blood was drawn by heart puncture into a heparinized syringe. Spleen, parathymic lymph nodes, leptomeninges and parenchyma of the spinal cord were dissected and homogenized by passing through a metal strainer. Lymphocytes were isolated from blood by a Nycoprep gradient. First, the blood was diluted with an equal volume of PBS and overlaid onto Nycoprep. After centrifugation at 800g, room temperature for 30 min with mild acceleration and brake, lymphocytes were collected from the interface. For spleen, erythrocytes were removed by treating with ACK buffer for 3 min on ice and CD4⁺ T cells were enriched using the EasySep Rat CD4⁺ T Cell Isolation Kit (StemCell technologies), before purification by sorting. From the spinal cord parenchyma, the lymphocytes were isolated using a 30%/64% Percoll gradient and centrifugation at 1,200g, room temperature for 30 min with mild acceleration and brake. Lymphocytes were collected from the interface.

Flow cytometry. For the CRISPR screens, BFP⁺ T_{MBP} cells were sorted from spleen only (genome-wide screen) or from all four tissues (validation screen) using a FACS Aria III (BD) or FACS Fusion (BD) with FACSDiva at the Flow Cytometry Core Facility of the Biomedical Center, LMU. Cells were sorted to achieve an sgRNA coverage of >100× (the same sgRNA being present in at least 100 sorted T cells). The expression of cell surface molecules was measured by flow cytometry after antibody labeling. T cells were incubated for 30 min on ice with the primary antibody diluted in FACS buffer (PBS with 1% rat serum and 0.05% NaN₃). After washing three times with FACS buffer, the cells were incubated with a fluorochrome-conjugated secondary antibody in FACS buffer for 30–45 min on ice. The following antibodies were used with a 1:100 dilution unless stated otherwise: Mouse IgG1 Isotype control (Sigma), Armenian hamster IgG2 Isotype control (BD), mouse anti-rat CD49d (Thermo Fisher), mouse anti-rat CD11a (BioLegend), mouse anti-rat CD18 (Thermo Fisher), mouse anti-rat TCRβ (BD), mouse anti-rat CD25 (Thermo Fisher), mouse anti-rat CD134 (Thermo Fisher), Armenian hamster anti-rat CD29 (BioLegend), APC conjugated donkey anti-mouse IgG (Jackson ImmunoResearch, 1:1,000 dilution), APC conjugated goat anti-Armenian hamster IgG (Jackson ImmunoResearch, 1:1,000 dilution) and AF647 conjugated goat anti-mouse IgG (SouthernBiotech, 1:1,000 dilution). Cells were then washed once in FACS buffer and once with PBS, then resuspended in PBS and analyzed by flow cytometry. For intracellular staining, T cells were incubated with 5 µM Brefeldin (Sigma Aldrich) in complete DMEM supplemented with 1% rat serum for 5 h at 37 °C and fixed with 2% paraformaldehyde for 20 min on ice. The T cells were stored in PBS at 4 °C until intracellular staining. The staining was performed similarly to the surface staining

with the following antibodies diluted in permeabilization buffer (Bio-Legend): mouse IgG1 Isotype control (Sigma), PE conjugated rat IgG1 isotype control (BD), mouse anti-rat IFN- γ (eBioscience), PE conjugated rat anti-mouse/rat IL-17A antibody (BD) and APC conjugated donkey anti-mouse IgG (Jackson ImmunoResearch). For assessment of in vivo migration and ex vivo cell surface molecule detection, BFP⁺ T_{MBP} cells and EGFP⁺ T_{MBP} cells were analyzed using a FACS VERSE (BD) with FACS Suite, LSRFortessa (BD) flow cytometer with FACSDiva or Cytoflex S with CytExpert (Beckman Coulter). For in vitro surface and intracellular staining, cells were analyzed with Cytoflex S.

For in vivo migration assays, the KO/control ratio based on the numbers of BFP⁺ or EGFP⁺ cells in the lymphocyte gate was calculated for all tissue samples and normalized to the blood ratio of the same animal (tissue KO cell number/control cell number ratio divided by the blood KO/control ratio in the same animal). Thus, the migration phenotype for the gene KO was always compared to the migration control T_{MBP} cells within that animal to correct for inter-animal and inter-experiment variability.

Next-generation sequencing sgRNA library preparation. Genomic DNA from lymphocytes or sorted T_{MBP} cells was isolated with the DNeasy Blood and Tissue Kit (Qiagen). A one-step PCR amplification was performed with Q5 High Fidelity DNA Polymerase by using 2.5 μ g of genomic DNA per reaction with Fwd-Lib (mix of eight staggered primers) and Rev-Lib (consists of 8 bp of unique barcode) primers for a total of 24 cycles. Illumina adaptors were introduced together with the amplification primers. All primer sequences are listed in Supplementary Table 3. The amplified DNA amplicons were purified with SPRIselect (Beckman Coulter) with a ratio of 1:0.8 (DNA to beads) and eluted in nuclease-free water. The presence of ~250-bp DNA amplicons was confirmed, and the concentration was measured with Agilent Bioanalyzer on DNA 1000 chips (5067-1504). Library samples were sent to The Laboratory for Functional Genome Analysis (LAFUGA) at the Gene Center Munich for sequencing single-end 50 bp on a HiSeq 1500.

qPCR and 3' bulk mRNA sequencing. All primer sequences are listed in Supplementary Table 3.

Total RNA from cells was isolated with either an RNeasy Plus Mini (Qiagen) or a Micro (Qiagen; for less than 100,000 cells) kit according to the manufacturer's protocol. For qPCR, cDNA was synthesized using the RevertAid H Minus First Strand cDNA synthesis kit (Thermo Fisher) with 100–500 ng total RNA and Oligo (dt) primers and assays were performed on the Bio-Rad CFX Connect Real-Time PCR system using SsoAdvanced Universal SYBR Green Supermix (Bio-Rad). The β -actin housekeeping gene was used to normalize the variability in expression level. All qPCR reactions were run in duplicates. Results were quantified using the $\Delta\Delta$ Ct method. For 3' bulk mRNA-seq, the library was prepared from total RNA using the Collibri 3' mRNA Library Prep Kits for Illumina Systems (Thermo Fisher). Amplification of transcripts was confirmed with an Agilent Bioanalyzer on DNA 1000 chips and sent to LAFUGA (Gene Center, LMU Munich) for single-end 50-bp sequencing on a HiSeq 1500.

Western blotting. For assessment of Phospho-ERK levels after stimulation of SIPRI1 signaling, T cells were incubated in medium consisting of 1 μ M SIP (Tocris) for 10 min at 37 °C. For all western blot analyses, T_{MBP} cells were washed twice with PBS and lysed with RIPA buffer (Thermo Fisher) including inhibitors of proteases (Sigma) and phosphatases (Sigma). Pierce Bovine Serum Albumin Standard Pre-Diluted Set Kit (Thermo Fisher) or Pierce Rapid Gold BCA Protein Assay Kit (Thermo Fisher) was used to calculate the protein concentration of samples. Lysates were boiled at 95 °C for 5 min in a mix with Tris-Glycine SDS sample buffer (Thermo Fisher) and reducing agent (Thermo Fisher). Lysates were resolved in 4–12% Tris-Glycine gels (Thermo Fisher) for protein separation and transferred to PVDF membrane (Millipore)

using Mini Gel Tank and Blot Module (Thermo Fisher). Anti-GRK2 (CST, 1:1,000 dilution), anti-phospho-p44/42 MAPK (ERK1/ERK2; Thr202/Tyr204; CST, 1:1,000 dilution), anti-p44/p42 MAPK (ERK1/ERK2; CST, 1:1,000 dilution), anti-ETS1 (CST, 1:1,000 dilution) and horseradish peroxidase-conjugated β -actin (Santa Cruz, 1:100,000 dilution) primary antibodies were incubated on the membrane overnight at 4 °C in 5% BSA-TBST buffer, followed by incubation with a horseradish peroxidase-conjugated secondary rabbit antibody (Santa Cruz, 1:10,000 dilution) at room temperature for 2 h. Blots were imaged using the LiCor Odyssey Fc system after treatment with ECL Western Blotting-Substrate (Thermo Fisher) or SuperSignal West Femto Maximum Sensitivity Substrate (Thermo Fisher) and analyzed with Image Studio Lite Software (LiCor)

Transwell chemotaxis assay. Chemotaxis assays were performed using a 96-well transwell chamber with a 5- μ m pore size (Corning). T cells were resuspended in complete DMEM supplemented with 1% rat serum. Control-BFP⁺ and KO-EGFP⁺ cells were counted and mixed at a ratio of 1:1. Each upper insert received 0.2×10^6 T cells in 75 μ l medium. To the lower compartment, 235 μ l of complete DMEM supplemented with 1% rat serum with or without chemotactic stimuli (30 ng ml⁻¹ CXCL10, PeproTech or CCL5, PeproTech) was added. The chemotaxis plates were centrifuged (400g, 1 min) and incubated at 37 °C with 10% CO₂ for 5 h. After incubation, migrated cells in the lower chamber were analyzed by flow cytometry using an LSRFortessa (BD) with FACSDiva or CytoFlex S with CytExpert (Beckman Coulter). For analysis and quantification, the percentage of cells detected in the lower chamber was normalized to input values. Then, the KO/control ratio was calculated for all conditions.

Intravital imaging of the spinal cord leptomeninges. Two or three days after intravenous co-transfer of 1×10^6 BFP⁺ control and 1×10^6 EGFP⁺ *Grk2*-KO T cells, intravital imaging within the spinal cord leptomeninges was performed as previously described⁶. The animal was anesthetized by intramuscular injection of MMF (2 mg per kg body weight midazolam, 150 μ g per kg body weight medetomidine and 5 μ g per kg body weight fentanyl), and a tracheotomy was performed to allow mechanical ventilation with 1.5–2.0% isoflurane in air. The body temperature of the animal was maintained by a heat pad placed underneath. Furthermore, a catheter was inserted into the tail vein to allow intravenous injection of Texas Red-conjugated 70-kDa dextran (100 μ g) to visualize blood plasma during the imaging. To allow imaging, a laminectomy was performed at the dorsal part of Th12/Th13. For this, the skin was opened with a midline incision of 3 cm and the paravertebral musculature on the spine was removed. Then the animal was fixed in a custom-made fixation device, which provides stability by pushing with three pins from one side to the spine. The dorsal part of the central spine disc was removed after cutting both sides using a dental drill. The dura was then removed. To avoid artifacts due to breathing, the animal was slightly lifted before starting imaging. Time-lapse images were acquired with a Leica SP8 microscope using a water-immersion $\times 25$ objective lens (numerical aperture of 1.00, working distance of 2.6 mm). For excitation of BFP and EGFP, a pulsed laser from an InSight DS+ Single (Spectra Physics) was adjusted to 840 nm, and fluorescence signals were first separated with a beam splitter (BS560). Signals of shorter wavelength were again split by BS505 and detected after the band-pass filters HC405/150 (BFP) and ET525/50 (EGFP). Signals of a longer wavelength were again separated by beam splitter RSR620 and detected after the band-pass filter BP585/40 (Texas Red). Images were acquired from a field of approximately 440 μ m \times 440 μ m with a resolution of 512 \times 512 pixels and an approximate 100 μ m z-stack, with an interval of 2–3 μ m.

The images were processed by Fiji. First, a Gaussian blur filter (cutoff of 1 pixel) was used, followed by maximum z-projection. When necessary, bleed-through liner subtraction was applied. Finally, signal

intensity was adjusted by linearly adjusting brightness and contrast. For tracking of the cells, the Manual Tracking Plugin of Fiji was used to obtain coordinates, which were used to calculate migration speed and distance of the cells in Excel together with information from imaging such as time and pixel resolution. Locations of cells were analyzed by the Cell Counter Plugin of Fiji.

CRISPR editing of human CD4⁺ T cells. Cells derived from leukoreduction system chambers were diluted at a 1:5 ratio with PBS and added to a SepMate tube containing human Pancoll. During centrifugation (1,200g for 10 min at 4 °C), PBMCs were isolated by density gradient. CD4⁺ human T cells were enriched from PBMCs using EasySep Human CD4⁺ T Cell Isolation Kit (StemCell Technologies) according to the manufacturer's protocol. CRISPR RNPs targeting control (NT), S1PR1-GRK2, ETS1, HSP90B1, CXCR3 and TBX21 were delivered into the CD4⁺ Human T cells by using Amaxa 4D-Nucleofector System and P2 Primary Cell 4D-Nucleofector X Kit S (Lonza) according to the manufacturer's instructions using the pulse code EH100 (ref. 58). Briefly, per reaction, 0.375 µl of Alt-R CRISPR-Cas9 tracrRNA (200 pmol µl⁻¹) and 0.375 µl of Alt-R CRISPR-Cas9 crRNA (200 pmol µl⁻¹) were mixed and the solution was then incubated at 95 °C for 5 min, decreasing to 70 °C at the rate of 0.5 °C s⁻¹, at 70 °C for 1 min, then allowed to cool to room temperature. Next, 5 µg Alt-R S.p. HiFi Cas9 Nuclease V3 (IDT) was mixed with crRNA:tracrRNA duplex and the mixture was incubated at room temperature for 20 min for RNP formation. After washing with PBS, 2 × 10⁶ T cells were pelleted and resuspended in 23 µl of P2 nucleofection buffer and mixed with RNP complex. Then, 0.8 µl of Alt-R Cas9 Electroporation Enhancer (stock solution of 100 µM; IDT) was added per reaction before the electroporation. RNP electroporated T cells were transferred to round-bottom 96-well plates (Corning) at a concentration of 1 × 10⁵ T cells per well in RPMI medium supplemented with Primocin (100 µg ml⁻¹; Invivogen) and 10% charcoal-stripped FBS (Thermo Fisher). For stimulation of T cells, the medium was additionally supplemented with monoclonal anti-CD3 (1 µg ml⁻¹; Thermo Fisher) and anti-CD28 (2 µg ml⁻¹; Thermo Fisher) for 72 h at 37 °C in an incubator. T cells were then washed and further incubated with recombinant human IL-2 (10 ng ml⁻¹; R&D systems) for up to 3 weeks in a 37 °C/5% CO₂ incubator with medium change every 3 d. All crRNA sequences are listed in Supplementary Table 3. For ETS1, HSP90B1, CXCR3 and TBX21 editing, CD4⁺ T cells between day 7 and day 21 after isolation were used. T cells were washed with PBS and stained with anti-CD4-FITC (BioLegend), anti-CXCR3-PE (BioLegend), anti-CD49d-APC (BioLegend), anti-CD11a-PE (BioLegend) and anti-CD29-PE (BioLegend) antibodies at a concentration of 1:100 and with LIVE/DEAD Violet dye (Thermo Fisher) at a 1:1,000 concentration for 30 min in FACS buffer (PBS with 1 mM EDTA and 1% charcoal-stripped FBS) and analyzed by flow cytometry using CytoFlex S with CytExpert (Beckman Coulter).

S1PR1 internalization assay with human CD4⁺ T cells. Charcoal-stripped FBS was used in the medium to prevent unwanted S1PR1 receptor internalization. Human CD4⁺ T cells between day 6 and day 13 after isolation were used for the S1PR1 internalization assay. T cells were incubated in control medium (with PBS containing 4% fatty-acid-free BSA (Sigma) used to dissolve SIP as vehicle) or medium consisting of either 1 µM SIP (Tocris) or 1 nM fingolimod-P (FTY720 Phosphate, Biomol) for 90 min at 37 °C. T cells were then washed with PBS and stained with anti-CD4-FITC (BioLegend) and anti-S1PR1-eF660 (Thermo Fisher) at a concentration of 1:100 and with LIVE/DEAD Violet dye (Thermo Fisher) at 1:1,000 concentration for 30 min in FACS buffer (PBS with 1 mM EDTA and 1% charcoal-stripped FBS). S1PR1 expression in CD4⁺ T cells was assessed by flow cytometry using CytoFlex S with CytExpert (Beckman Coulter).

Collection and processing of human samples for single-cell transcriptomics. *Peripheral blood mononuclear cells.* After collection of

blood into tubes containing EDTA, samples were diluted at a 1:1 ratio with PBS and added to a SepMate tube containing human Pancoll. During centrifugation (1,200g for 10 min at 4 °C), PBMCs were isolated by density gradient. The isolated cells in plasma were transferred to a tube and centrifuged again at 300g for 10 min at 4 °C. The isolated PBMCs were either used freshly or cryopreserved in liquid nitrogen, using serum-free cryopreservation medium (CTL-Cryo ABC Media Kit, Immunospot).

For analysis, samples were thawed quickly, washed twice with 1% BSA/PBS (300g for 10 min at 4 °C) and labeled using the following procedure: 10 min at 4 °C with Fc-block (Miltenyi) at a 1:50 dilution in FACS buffer (PBS + 2% FBS), followed by the surface antibody mix. The mix comprised: Thermo Fisher anti-human CD45RO-FITC (1:40 dilution), anti-CCR7-APC (1:40 dilution), anti-CD3-AF700 (1:50 dilution), Fixable Viability Dye eFluor 780 (1:1,000 dilution), anti-CD4-Pacific Blue (1:25 dilution) and BioLegend: anti-CD8-PerCP (1:25 dilution), in a total volume of 100 µl FACS buffer and incubated for 30 min at 4 °C. Antigen-experienced CD4⁺ T cells consisting of CD3⁺CD4⁺CD8⁻ effector memory (CD45RO⁺CCR7⁻), effector (CD45RO⁻CCR7⁻) and central memory (CD45RO⁺CCR7⁺) cells were collected using a FACS Aria Fusion flow cytometer with FACSDiva (BD Biosciences). After, cells were washed in 0.04% BSA/PBS and approximately 16,500 cells per sample were loaded onto the 10x chip.

Cerebrospinal fluid. Human CSF samples (3–6 ml) were processed within 1 h of lumbar puncture. After centrifugation at 300g for 10 min, the cell pellet was incubated in a 2-ml tube with the following TotalSeq-C antibodies: anti-human CD4, anti-CD8A and mouse IgG1 isotype control (BioLegend, 0.5 µg of each). Then, we followed the Cell Surface Labeling Protocol from 10x Genomics, but with all centrifugations done at 300g for 10 min. All cells were loaded on the 10x chip, with a maximum target cell number of 10,000.

10x library preparation and sequencing. Further processing was done following the manufacturer's protocol using the Chromium Next GEM Single Cell VDJ v1.1. For CSF samples, the Feature Barcoding technology for Cell Surface Protein steps was also performed. Libraries were sequenced on an Illumina NovaSeq 6000 S4 using the following read lengths: 150 bp, read 1; 8 bp, i7 index; 150 bp, read 2.

Bioinformatic analysis. CRISPR screen analysis. The Galaxy platform⁵⁹ was used for data analysis. For raw fastq files, Je-Demultiplex-Illu (Galaxy Version 1.2.1) was used for de-multiplexing, followed by Cutadapt (Galaxy version 4.4+galaxy0) and Trimmomatic (Galaxy Version 0.39+galaxy0) to get the 20-bp sgRNA sequence. Counts were then obtained with MAGeCK²⁰ (version 0.5.7.1) count. Normalization across samples was conducted in R⁶⁰ (version 4.0.0+) after a 50 raw count threshold using the geometric mean per sgRNA for normalization, and sgRNAs with fewer than 50 counts in more than two replicates of the same tissue were discarded altogether. The MAGeCK test was run without normalization or zero removal, and otherwise default parameters on Galaxy, using the information of control NT sgRNA for noise correction. All further data processing was done with R.

Genome-wide screen analysis and validation screen design. For plotting of the control values in genome-wide analysis results (Fig. 1b and Extended Data Figs. 1 and 2), four random control sgRNAs were sampled with replacement from the control sgRNA pool and their log₂(fold change) averaged, for a total of 800 combinations of control 'genes' with four different sgRNAs each, to model the variability observed for a control 'gene' in the MAGeCK analysis.

The selection of candidates for the validation screen was performed based on the MAGeCK results of the genome-wide screen. All genes in meninges versus blood and parenchyma versus blood comparisons with an absolute 'neg|lfc' or 'pos|lfc' > 0.5 were included. Genes from other comparisons (meninges or parenchyma versus spleen and spleen versus blood) were included when the absolute 'neg|lfc' or 'pos|lfc' > 1 and the number of 'neg|goodsgrna' ≥ 2 for negative

'neg|lfc' candidates or of 'pos|goodsgrna' ≥ 2 for positive 'pos|lfc' candidates, or the absolute 'neg|lfc' or 'pos|lfc' > 0.6 and the number of 'neg|goodsgrna' or 'pos|goodsgrna' > 2 . Only genes expressed in T cells (based on ref. 7) were included for validation, except for genes from meninges or parenchyma versus blood if they had an absolute 'neg|lfc' or 'pos|lfc' > 0.85 . In addition to the genes selected based on these criteria, we also included genes expressed in T cells (based on ref. 7) belonging to the GO terms [GO:0004896](#) (cytokine receptor activity), [GO:0050840](#) (extracellular matrix binding), [GO:0004930](#) (GPCR activity), [GO:0005178](#) (integrin binding) and [GO:0033627](#) (cell adhesion mediated by integrin). We further included genes from selected gene sets from running GSEA (Broad) with default parameters except for 'metric for ranking genes' = 'log₂ Ratio of Classes', databases of the GSEA molecular signature databases v7.0, and maximum and minimum sizes for excluding gene sets 20,000 and 5, respectively. The selected gene sets were [GO:0043112](#) (receptor metabolic process), [GO:0072583](#) (clathrin-dependent endocytosis), [GO:0097384](#) (cellular lipid biosynthetic process), [GO:0042092](#) (type 2 immune response), [GO:0051955](#) (regulation of amino acid transport), [GO:0098661](#) (inorganic anion transmembrane transport), [GO:0015698](#) (inorganic anion transport), [GO:0035655](#) (IL-18-mediated signaling pathway), [GO:0071277](#) (cellular response to calcium ion), [GO:0016574](#) (histone ubiquitination), [GO:0043968](#) (histone H2A acetylation), [GO:0006089](#) (lactate metabolic process), [GO:0070670](#) (response to IL-4), [GO:0032606](#) (type I interferon production) and [GO:0002755](#) (MyD88-dependent toll-like receptor signaling pathway). For some GO terms, only the genes having a negative log₂(fold change) when the GO term was negatively enriched or positive log₂(fold change) when the GO term was positively enriched were included. This resulted in a total of 1,374 genes that were selected based on log₂(fold change) and significance cutoffs in different comparisons and 587 genes that were selected based on GO terms, for a total of 1,961 genes (Supplementary Table 3).

Identification of essential regulators of migration. Validation screen candidates were considered essential regulators of T cell migration to the CNS when they met the following criteria as per the results of the MAGeCK analysis: 'neg|lfc' < -3 times the standard deviation of control (NT) 'neg|lfc' and 'pos|lfc' in the sample, the number of 'neg|goodsgrna' ≥ 3 , and the 'neg|p-value' < 0.05 ; or 'pos|lfc' > 3 times the standard deviation of control 'neg|lfc' and 'pos|lfc' in the sample, the number of 'pos|goodsgrna' ≥ 3 and the 'pos|p-value' < 0.05 .

Bulk RNA-sequencing data. Galaxy and R were also used for bulk RNA-seq data processing. Fastq files were aligned with RNA STAR (version 2.7.2b) to the reference genome Rnor_6.0.102 with default parameters and without trimming. HTSeq-count (version 1.0.0) was then used, and differential expression determined with DESeq2 (version 2.11.40.7+galaxy1), with 'estimateSizeFactors' = poscounts and otherwise default parameters. Batch correction per animal was performed when applicable. All further analysis was run with R, tidyverse^{60,61} (version 4.0.0+). For pathway analysis, the gProfiler⁶² web tool was used on genes with an adjusted *P* value < 0.05 in an ordered query from most to least extreme log₂(fold change).

Processing of single-cell sequencing data. Sequencing results were de-multiplexed and aligned to the human GRCh38 reference genome using Cell Ranger (10X Genomics, v.6.1). Gene barcodes with unique molecular identifier counts that reached the threshold for cell detection were included in subsequent data analysis, using the R package Seurat⁶³ (version 4.1.0).

Analysis of human scRNA-seq data within compartments. In a first step, data from the different compartments were analyzed separately. Data from cells with between 200 and 5,000 genes per cell and a percentage of mitochondrial genes below 10% were included in further analyses. Genes expressed in fewer than three cells were excluded. Data were log normalized and a batch effect was found in both the CSF and blood compartments. Therefore, established integration methods implemented within the Seurat package (CCA (canonical correlation

analysis) and rPCA (reciprocal principal component analysis)) were applied, using the vst algorithm for detection of variable features. Data were then scaled and principal components computed for dimensional reduction. Applying *k*-nearest neighbors, the neighborhood overlap between cells was computed, followed by clustering the cells with a shared nearest-neighbor-based clustering algorithm. Uniform manifold approximation and projection was applied to visualize data in a two-dimensional space. The information from TCR enrichment library sequencing (10x Genomics, v.6.1) was added for each cell, followed by subsetting for cells where a TCR clonotype and only one beta chain had been detected. Small cell clusters with low quality and doublets, as well as a cluster expressing natural killer T cell signatures, were removed. For selecting the CD4⁺ T cells of the CSF for further analysis, the information provided by the anti-CD4 staining was used.

Computing the TCR overlap between compartments. For each individual MS or control sample, the amino acid sequence information from the TCR enrichment sequencing was used to match cells with identical TCR expression present in both the blood and CSF compartment of the same participant. If the expression of a TCR was found across compartments, cells were considered as overlapping. For TCRs found more or equal three times in total, cells were labeled as expanded across tissues.

Combined analysis of human scRNA-seq data. Both datasets (CSF and blood) were merged, log normalized, integrated with rPCA and scaled, before undergoing principal component analysis, neighborhood computation, clustering and dimensionality reduction using uniform manifold approximation and projection. The remaining 13 clusters were assigned a number, based on their expression level of CCR7 from high to low, with a Treg cluster characterized by Foxp3 expression. Each of the clusters expressed specific features, making them distinct on a transcriptomic level (Extended Data Fig. 8). Cluster T12 included only 13 cells from the CSF and was manually assigned to the nearest cluster T7 as it appeared to be unique for the blood compartment.

Pathway analysis of human scRNA-seq data. For analysis of enriched pathways in overlapping T cells compared to nonoverlapping cells derived from the blood of participants with MS (Extended Data Fig. 9), differentially expressed genes were computed using the R package MAST90 within the FindMarkers function of Seurat, with 'logfc.threshold' = 0, per cluster and overall. Genes enriched in overlapping versus nonoverlapping cells with an 'avg_log2FC' > 2 times the standard deviation of the 'avg_log2FC' of the individual comparison and a 'p_val_adj' < 0.05 were subset and the package EnrichR⁶⁴⁻⁶⁶ was used for pathway analysis using the database 'GO_Biological_Process_2021'. Pathways with an 'Adjusted.P.value' < 0.05 and 'Count' ≥ 2 were considered significant and included in further analysis. For Extended Data Fig. 9c, the pathways plotted are derived from the comparison of all overlapping versus nonoverlapping cells (not taking into account the clusters), but only pathways that were enriched in overlapping cells compared to nonoverlapping cells in the overall comparison as well as in at least five other individual cluster-specific comparisons were included in the plot.

Schematic representation of functional modules. For Figs. 2i, 3g and 4j, the schematic representations of the essential modules regulating T cell migration were composed based on published studies, for the adhesion module^{27,67-84}, for the chemotaxis module^{22,30,85-88} and for the egress module^{33,89-93}. Color coding corresponds to parenchyma versus blood log₂(fold change) values derived from the validation screen for those genes included in this screen (Supplementary Table 2); if the gene was not included due to not passing the initial selection criteria, color coding corresponds to the parenchyma versus blood log₂(fold change) values derived from the genome-wide screen (Supplementary Table 1). For genes with more than one isoform, only those deemed relevant based on the literature are shown. When there were no published reports, only the isoforms included in the validation screen and thus

showing a more pronounced \log_2 (fold change) in the genome-wide screen were included. All parenchyma versus blood values used to generate the figures can be found in Supplementary Table 4.

Statistical analysis and software. FlowJo (version 10+) was used for analysis of flow cytometry data. For statistical analyses and plotting, GraphPad Prism version 7+ (GraphPad Software) and R^{60,61} (version 4.0.0+) were used. Calculations for total cell numbers were performed using R and Excel (Microsoft Office). Data are represented as the mean \pm s.d. In box-and-whisker plots (Figs. 2, 3 and 4), the line in the middle of the box is the median, the box extends from 25th to 75th percentiles, whiskers extend from minimum to maximum values and the line connecting the box-and-whisker plots represents the mean. Sample sizes are reported in the figure legends. All replicates are biological. Measurements were not repeated except in clinical-course experiments, where the same animal was tracked across several days. For disease-course experiments, the control animals were selected based on the same date of the cell transfer as for the KO-transferred animals. Some control animals in the disease-course analysis were therefore used for more than one KO. KO/control comparisons are represented as a ratio KO phenotype/control phenotype, unless otherwise specified. For the *Grk2*-KO/*Slpr1*-KO and double-KO experiment, the *Grk2*-KO values are the same as depicted previously for the *Grk2*-KO migration phenotype data (Fig. 4b,i). For in vitro surface staining experiments and intracellular cytokine stainings, control values are reused and therefore identical across different figures (Extended Data Figs. 4–7) as specified in the legends. The Shapiro–Wilk normality test was used to determine Gaussian distributions. When the dataset showed a Gaussian distribution, parametric tests were applied; in cases of a non-Gaussian distribution, non-parametric tests were used. The statistical analysis of CRISPR screen results was performed solely with the MAGeCK software²⁰ using default settings (Figs. 1, 2, 3 and 4, Extended Data Figs. 1, 2 and 3 and Supplementary Tables 1, 2 and 4) and RNA-seq statistical analysis was performed solely by DESeq2 (galaxy; Fig. 6 and Extended Data Figs. 6 and 7), as described above. Test statistics were corrected for multiple testing if more than one comparison was run in parallel, with a two-stage linear step-up procedure of Benjamini, Krieger and Yekutieli. For the evaluation of KO T_{MBP} cell migration validation experiments by FACS, animals with <100 cells detected in any population were excluded. All KO/control phenotype datasets were statistically evaluated with one-sample *t*-tests (parametric) or Wilcoxon signed-rank tests (non-parametric). For the *Grk2*/*Slpr1*-KO experiment, an ordinary one-way ANOVA with Tukey's multiple-comparison tests (parametric) and Kruskal–Wallis test with Dunn's multiple-comparison test (non-parametric) were run for the KO/control phenotypes across the different KOs. For the assessment of the disease induction and weight change phenotypes of the KO cell transfer, a repeated-measures two-way ANOVA for time and genotype variations (days 3 to 8 after T_{MBP} cell transfer for disease score, and days 0 to 8 for weight changes) and Sidak's multiple-comparison test were run. For surface and intracellular FACS staining experiments, two-way ANOVAs were run with multiple comparisons between control and KO cells, correcting for multiple comparisons with the two-stage set-up method of Benjamini, Krieger and Yekutieli for controlling for the false discovery rate. The statistical tests are reported in the figure legends, as well as two-way ANOVA *F* and *P* values corresponding to T_{MBP} cell genotype variation (one degree of freedom), KO T_{MBP} cells compared to control T_{MBP} cells. All other *F* and *P* values are not reported. All statistical tests and *P* values are two tailed. For the human data, differential expression of genes between MS and control conditions and blood and CSF were computed using the R package MAST90 within the FindMarkers function of Seurat (Fig. 7 and Extended Data Figs. 9 and 10). Correlations are Pearson correlations, as indicated in the figure legends. Both CRISPR screens have three replicates. One blood replicate from the genome-wide screen was excluded due to bad technical quality. The bulk RNA-seq for the *Ets1*-KO and *Grk2*-KO experiments have three replicates. All other *n* values are

reported in the figure legends. Significance was set as: NS, $P > 0.05$; * $P < 0.05$, ** $P < 0.01$, *** $P < 0.001$ and **** $P < 0.0001$. Adobe Illustrator (Adobe Systems), Inkscape and PowerPoint (Microsoft Office) were used for figure preparation.

Sample size, randomization and blinding. For the CRISPR screens, the sample size was determined based on the number of cells needed to maintain a minimum of 100 \times and a maximum of 1,000 \times coverage in all relevant cell populations, with the aim to minimize false discovery rates and ensure statistically meaningful data while also considering the practicality of handling the required number of cells. The number of replicates was chosen based on ref. 94.

No statistical methods were used to predetermine sample sizes, but our sample sizes are similar to those reported in previous publications (refs. 5–7,18). For the analysis of human CD4⁺ T cells by NGS, the samples from MS and control participants were selected due to availability of sufficient biomaterials.

The animals were allocated randomly for experimental groups. Data collection and analysis were not performed blind to the conditions of the experiments.

Reporting summary

Further information on research design is available in the Nature Portfolio Reporting Summary linked to this article.

Data availability

NGS raw data and processed gene expression data that support the findings of this study are deposited in the Gene Expression Omnibus under the accession number [GSE232344](https://www.ncbi.nlm.nih.gov/geo/query/acc.cgi?acc=GSE232344) ([GSE232340](https://www.ncbi.nlm.nih.gov/geo/query/acc.cgi?acc=GSE232340) for data on the CRISPR screens, [GSE232339](https://www.ncbi.nlm.nih.gov/geo/query/acc.cgi?acc=GSE232339) for bulk RNA-seq data and [GSE232343](https://www.ncbi.nlm.nih.gov/geo/query/acc.cgi?acc=GSE232343) for scRNA-seq data). Source data are provided with this paper. All other data generated or analyzed during this study are included in the published article or are available from the corresponding authors upon reasonable request.

Code availability

Custom code used for the analysis of the data for this paper is available as Supplementary Code 1–5.

References

- Flügel, A., Willem, M., Berkowicz, T. & Wekerle, H. Gene transfer into CD4⁺ T lymphocytes: green fluorescent protein-engineered, encephalitogenic T cells illuminate brain autoimmune responses. *Nat. Med.* **5**, 843–847 (1999).
- Koike-Yusa, H., Li, Y., Tan, E. P., Velasco-Herrera, M. D. C. & Yusa, K. Genome-wide recessive genetic screening in mammalian cells with a lentiviral CRISPR-guide RNA library. *Nat. Biotechnol.* **32**, 267–273 (2014).
- Doench, J. G. et al. Optimized sgRNA design to maximize activity and minimize off-target effects of CRISPR–Cas9. *Nat. Biotechnol.* **34**, 184–191 (2016).
- Sanson, K. R. et al. Optimized libraries for CRISPR–Cas9 genetic screens with multiple modalities. *Nat. Commun.* **9**, 5416 (2018).
- Conant, D. et al. Inference of CRISPR edits from Sanger trace data. *CRISPR J.* **5**, 123–130 (2022).
- Seki, A. & Rutz, S. Optimized RNP transfection for highly efficient CRISPR/Cas9-mediated gene knockout in primary T cells. *J. Exp. Med.* **215**, 985–997 (2018).
- Afgan, E. et al. The Galaxy platform for accessible, reproducible and collaborative biomedical analyses: 2018 update. *Nucleic Acids Res.* **46**, W537–W544 (2018).
- R Core Team. R: a language and environment for statistical computing. R Foundation for Statistical Computing. <https://www.R-project.org/> (2021).

61. Wickham, H. et al. Welcome to the Tidyverse. *J. Open Source Softw.* **4**, 1686 (2019).
62. Raudvere, U. et al. g:Profiler: a web server for functional enrichment analysis and conversions of gene lists (2019 update). *Nucleic Acids Res.* **47**, W191–W198 (2019).
63. Hao, Y. et al. Integrated analysis of multimodal single-cell data. *Cell* **184**, 3573–3587 (2021).
64. Kuleshov, M. V. et al. Enrichr: a comprehensive gene set enrichment analysis web server 2016 update. *Nucleic Acids Res.* **44**, W90–W97 (2016).
65. Chen, E. Y. et al. Enrichr: interactive and collaborative HTML5 gene list enrichment analysis tool. *BMC Bioinformatics* **14**, 128 (2013).
66. Xie, Z. et al. Gene-set knowledge discovery with Enrichr. *Curr. Protoc.* **1**, e90 (2021).
67. De Bruyn, K. M. T., Rangarajan, S., Reedquist, K. A., Figdor, C. G. & Bost, J. L. The small GTPase Rap1 is required for Mn(2⁺)- and antibody-induced LFA-1- and VLA-4-mediated cell adhesion. *J. Biol. Chem.* **277**, 29468–29476 (2002).
68. Lu, L. et al. Kindlin-3 is essential for the resting $\alpha 4\beta 1$ integrin-mediated firm cell adhesion under shear flow conditions. *J. Biol. Chem.* **291**, 10363–10371 (2016).
69. Manevich-Mendelson, E. et al. Loss of kindlin-3 in LAD-III eliminates LFA-1 but not VLA-4 adhesiveness developed under shear flow conditions. *Blood* **114**, 2344–2353 (2009).
70. Franco, S. J. et al. Calpain-mediated proteolysis of talin regulates adhesion dynamics. *Nat. Cell Biol.* **6**, 977–983 (2004).
71. Carragher, N. O. & Frame, M. C. Focal adhesion and actin dynamics: a place where kinases and proteases meet to promote invasion. *Trends Cell Biol.* **14**, 241–249 (2004).
72. Lock, J. G., Wehrle-Haller, B. & Strömblad, S. Cell-matrix adhesion complexes: master control machinery of cell migration. *Semin. Cancer Biol.* **18**, 65–76 (2008).
73. Parsons, J. T., Horwitz, A. R. & Schwartz, M. A. Cell adhesion: integrating cytoskeletal dynamics and cellular tension. *Nat. Rev. Mol. Cell Biol.* **11**, 633–643 (2010).
74. Coló, G. P. et al. Focal adhesion disassembly is regulated by a RIAM to MEK-1 pathway. *J. Cell Sci.* **125**, 5338–5352 (2012).
75. Zaidel-Bar, R., Milo, R., Kam, Z. & Geiger, B. A paxillin tyrosine phosphorylation switch regulates the assembly and form of cell-matrix adhesions. *J. Cell Sci.* **120**, 137–148 (2007).
76. Zamir, E. & Geiger, B. Molecular complexity and dynamics of cell-matrix adhesions. *J. Cell Sci.* **114**, 3583–3590 (2001).
77. Ghandour, H., Cullere, X., Alvarez, A., Lusinskas, F. W. & Mayadas, T. N. Essential role for Rap1 GTPase and its guanine exchange factor CalDAG-GEF1 in LFA-1 but not VLA-4 integrin mediated human T-cell adhesion. *Blood* **110**, 3682–3690 (2007).
78. Lin, C. D. et al. Fever promotes T lymphocyte trafficking via a thermal sensory pathway involving heat shock protein 90 and $\alpha 4$ integrins. *Immunity* **50**, 137–151 (2019).
79. Hogg, N., Patzak, I. & Willenbrock, F. The insider's guide to leukocyte integrin signalling and function. *Nat. Rev. Immunol.* **11**, 416–426 (2011).
80. Han, J. et al. Reconstructing and deconstructing agonist-induced activation of integrin $\alpha 11\beta 3$. *Curr. Biol.* **16**, 1796–1806 (2006).
81. García-Bernal, D. et al. Vav1 and Rac control chemokine-promoted T lymphocyte adhesion mediated by the integrin $\alpha 4\beta 1$. *Mol. Biol. Cell* **16**, 3223–3235 (2005).
82. García-Bernal, D. et al. Chemokine-induced Zap70 kinase-mediated dissociation of the Vav1-talin complex activates $\alpha 4\beta 1$ integrin for T cell adhesion. *Immunity* **31**, 953–964 (2009).
83. Dios-Esponera, A. et al. Positive and negative regulation by SLP-76/ADAP and Pyk2 of chemokine-stimulated T-lymphocyte adhesion mediated by integrin $\alpha 4\beta 1$. *Mol. Biol. Cell* **26**, 3215–3228 (2015).
84. García-Bernal, D. et al. RGS10 restricts upregulation by chemokines of T cell adhesion mediated by $\alpha 4\beta 1$ and $\alpha 11\beta 3$ integrins. *J. Immunol.* **187**, 1264–1272 (2011).
85. Karin, N. CXCR3 Ligands in cancer and autoimmunity, chemoattraction of effector T cells, and beyond. *Front. Immunol.* **11**, 976 (2020).
86. Dar, W. A. & Knechtle, S. J. CXCR3-mediated T-cell chemotaxis involves ZAP-70 and is regulated by signalling through the T-cell receptor. *Immunology* **120**, 467–485 (2007).
87. Smit, M. J. et al. CXCR3-mediated chemotaxis of human T cells is regulated by a Gi- and phospholipase C-dependent pathway and not via activation of MEK/p44/p42 MAPK nor Akt/PI-3 kinase. *Blood* **102**, 1959–1965 (2003).
88. Richmond, A. & Nf-kappa, B. chemokine gene transcription and tumour growth. *Nat. Rev. Immunol.* **2**, 664–674 (2002).
89. Luo, J. & Benovic, J. L. G-protein-coupled receptor kinase interaction with Hsp90 mediates kinase maturation. *J. Biol. Chem.* **278**, 50908–50914 (2003).
90. Carlson, C. M. et al. Kruppel-like factor 2 regulates thymocyte and T cell migration. *Nature* **442**, 299–302 (2006).
91. Pyne, N. J. & Pyne, S. Sphingosine 1-phosphate receptor 1 signaling in mammalian cells. *Molecules* **22**, 344 (2017).
92. Willinger, T., Ferguson, S. M., Pereira, J. P., De Camilli, P. & Flavell, R. A. Dynamin 2-dependent endocytosis is required for sustained S1PR1 signaling. *J. Exp. Med.* **211**, 685–700 (2014).
93. Hwang, I.-Y., Park, C., Harrison, K. & Kehrl, J. H. Biased S1PR1 signaling in B cells subverts responses to homeostatic chemokines, severely disorganizing lymphoid organ architecture. *J. Immunol.* **203**, 2401–2414 (2019).
94. Ong, S. H., Li, Y., Koike-Yusa, H. & Yusa, K. Optimised metrics for CRISPR-KO screens with second-generation gRNA libraries. *Sci. Rep.* **7**, 7384 (2017).

Acknowledgements

We thank A. Schmalz, J. Schmitt and B. Fiedler for excellent technical assistance, and D. Matzek, B. Stahr and N. Ntaraklitsas for animal husbandry. We further thank H. Wekerle and R. Hohlfeld for critical reading of the manuscript, L. Robinson of Insight Editing London for critical review of the manuscript and F. Mayor and P. Penela for helpful input on the role of GRK2. We thank LAFUGA (Stefan Krebs, Helmut Blum) and CCGA Kiel (Sören Franzenburg, Janina Fuß) for NGS, the Core Facility Flow Cytometry at the BMC (L. Richter, P. Khosravani) for supporting flow cytometry and cell sorting, the Core Facility Bioimaging at the BMC (S. Dietzel, A. Thomae) for supporting the in vivo microscopy experiments and the LMU Biozentrum Sequencing Service for Sanger sequencing. This work was supported by a grant from the Deutsche Forschungsgemeinschaft (DFG) to N.K. and M.K. (Collaborative Research Center -TRR128, Project B10). Work in the laboratory of M.K. is further supported by the DFG via TRR 274/1 2020 (Projects C02, C05, Z01 – ID 408885537), TRR 152 (Project P27 – ID 239283807) and the Munich Cluster for Systems Neurology (SyNergy EXC 2145 – ID 390857198) as well as the ‘Klaus-Faber Stiftung’ and the ‘Verein Therapieforschung für MS-Kranke e.V.’. N.K. is further supported by a research grant from the DFG (ID 246754395) as are K.D., T.K. and E.B. (DO420/7-1). C.D.R. received support from the Fundación Rafael del Pino and is part of the DFG-funded Graduate School of Systemic Neurosciences (GSC 82 – ID 24184143). The funders had no role in study design, data collection and analysis, decision to publish or preparation of the manuscript.

Author contributions

M.K., N.K., K.F.L., C.D.R. and A.K. conceived and designed the experiments. A.K. and C.D.R. performed and evaluated CRISPR screening and editing. N.K., K.F.L. and L.Z. performed and evaluated T cell transfer experiments, in vitro migration assays and flow cytometry

analysis. N.K. and I.J.B. performed and analyzed in vivo spinal cord imaging. L.A.G. and T.K. collected and characterized MS participant and control samples. S.W. and C.W. contributed to collecting PBMCs and A.K. performed CRISPR editing of human T cells. K.E., V.K., K.D., C.D.R. and E.B performed and evaluated the single-cell transcriptomic analysis. M.K. wrote the paper with input from all authors.

Competing interests

The authors declare no competing interests.

Additional information

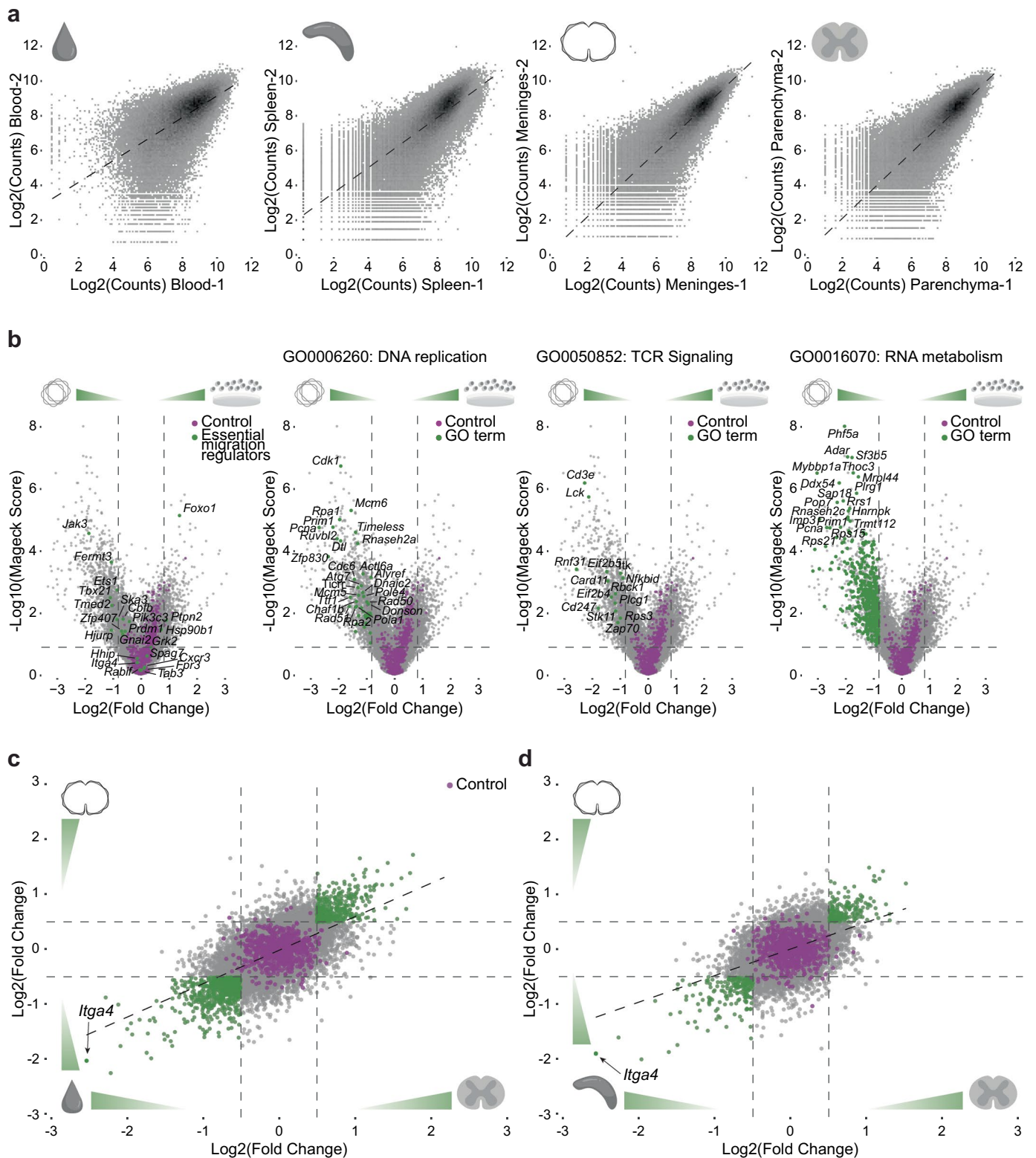
Extended data is available for this paper at <https://doi.org/10.1038/s41593-023-01432-2>.

Supplementary information The online version contains supplementary material available at <https://doi.org/10.1038/s41593-023-01432-2>.

Correspondence and requests for materials should be addressed to Martin Kerschensteiner or Naoto Kawakami.

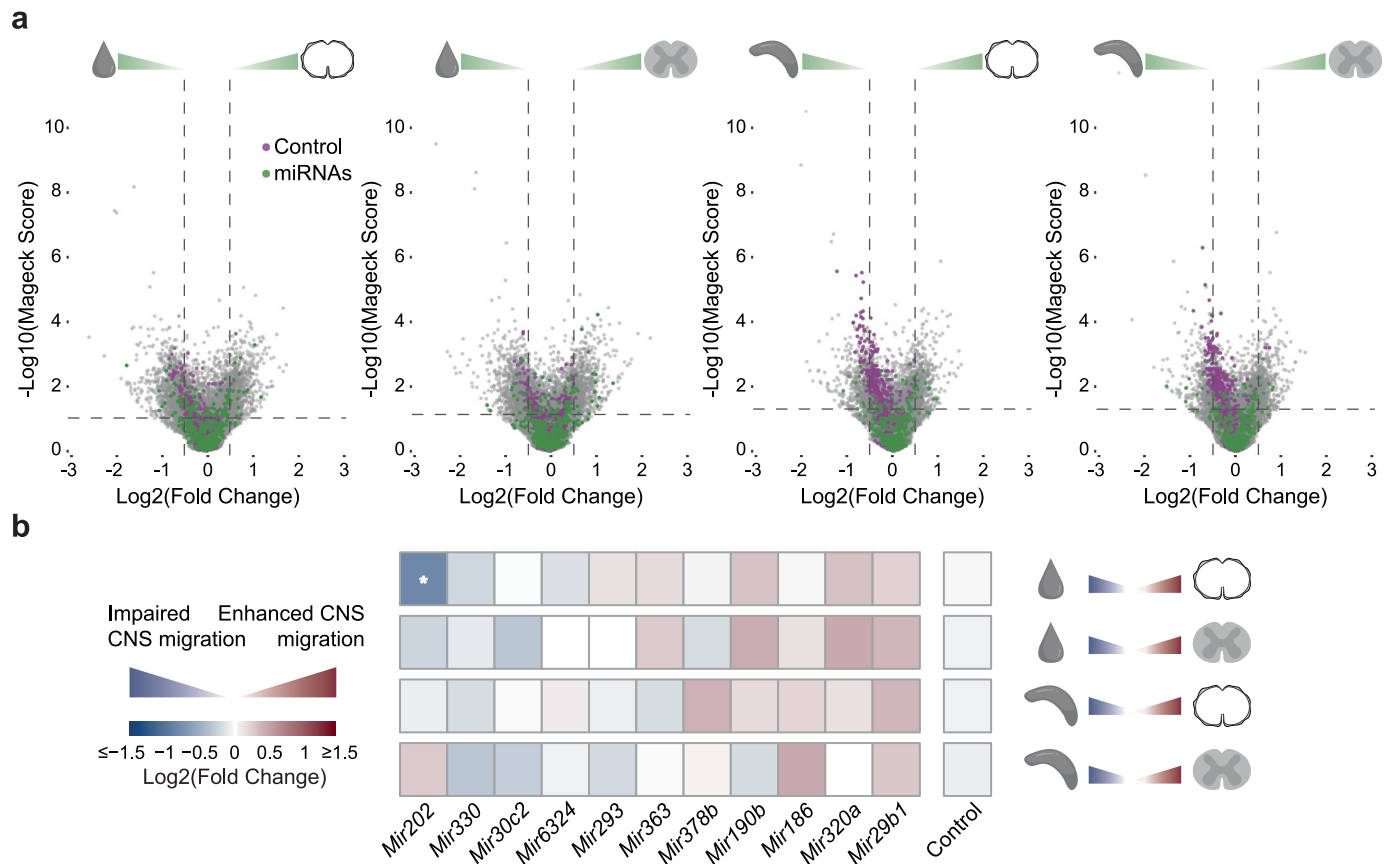
Peer review information *Nature Neuroscience* thanks Adrian Liston and the other, anonymous, reviewer(s) for their contribution to the peer review of this work.

Reprints and permissions information is available at www.nature.com/reprints.



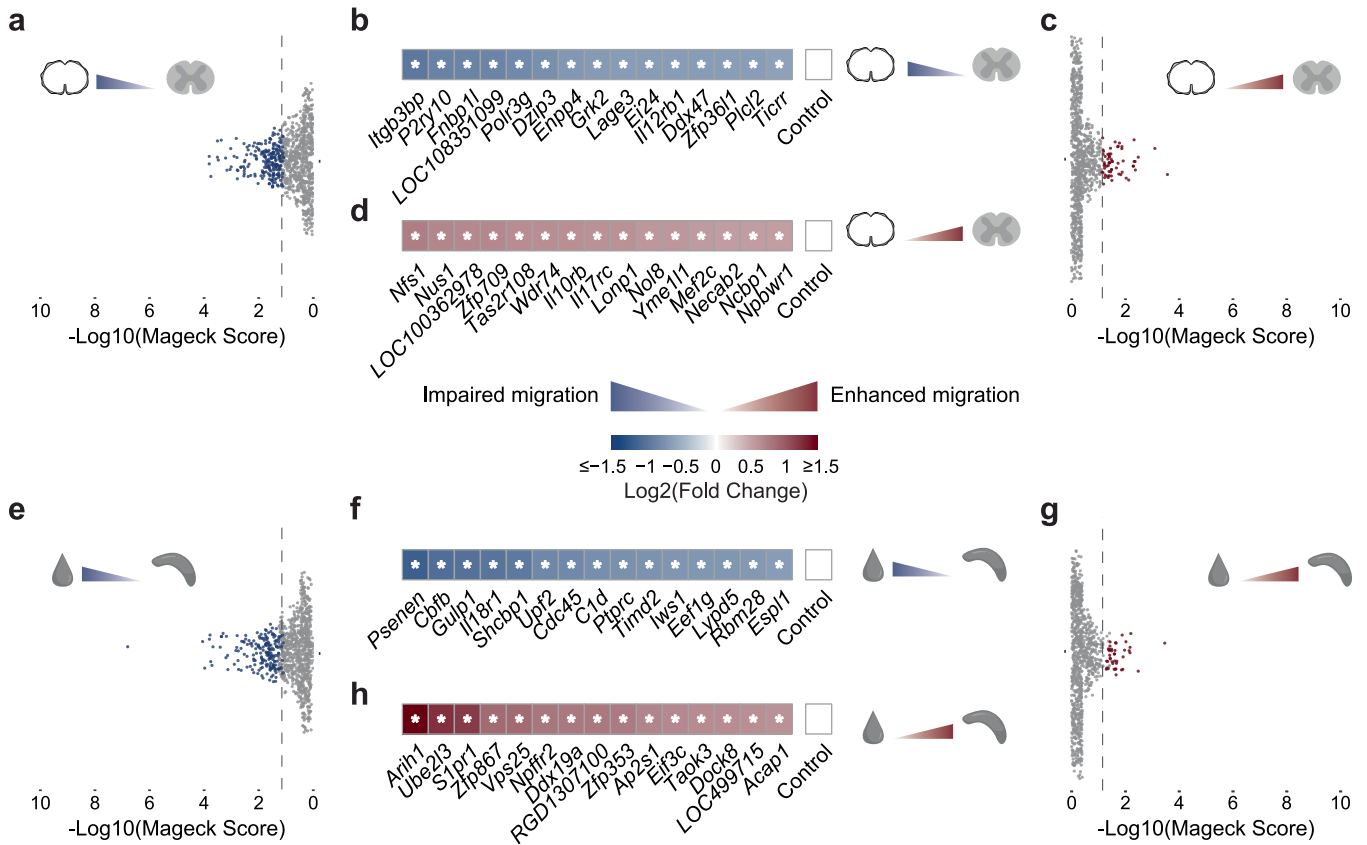
Extended Data Fig. 1 | Analysis of the genome-wide CRISPR screen. a. Correlations of the raw sgRNA count values of two representative replicates in (left to right) blood (Pearson correlation index of 0.74), spleen (0.78), meninges (0.86) and parenchyma (0.85). **b.** Volcano Plots of the genome-wide screen results comparing cultured TMBP cells right before in vivo transfer to the plasmid library, showing in green from left to right the essential regulators of migration as per Fig. 1d,f and genes belonging to the GO terms “DNA replication”, “TCR signaling” and “RNA metabolism”, many of which are depleted in cultured T cells

compared to the plasmid library. Lilac, controls. Lines indicate p-value = 0.05 and $\log_2(\text{Fold Change}) = \pm 3$ times the standard deviation of the controls. **c.** Correlation of $\log_2(\text{Fold Change})$ of genome-wide CRISPR screen for meninges vs. blood compared to parenchyma vs. blood (Pearson correlation index 0.62) and **d.** meninges vs. spleen compared to parenchyma vs. spleen (0.48). Green, correlating genes whose KO shows a sizeable change in the ability of TMBP cells to migrate into the CNS. Lilac, controls.



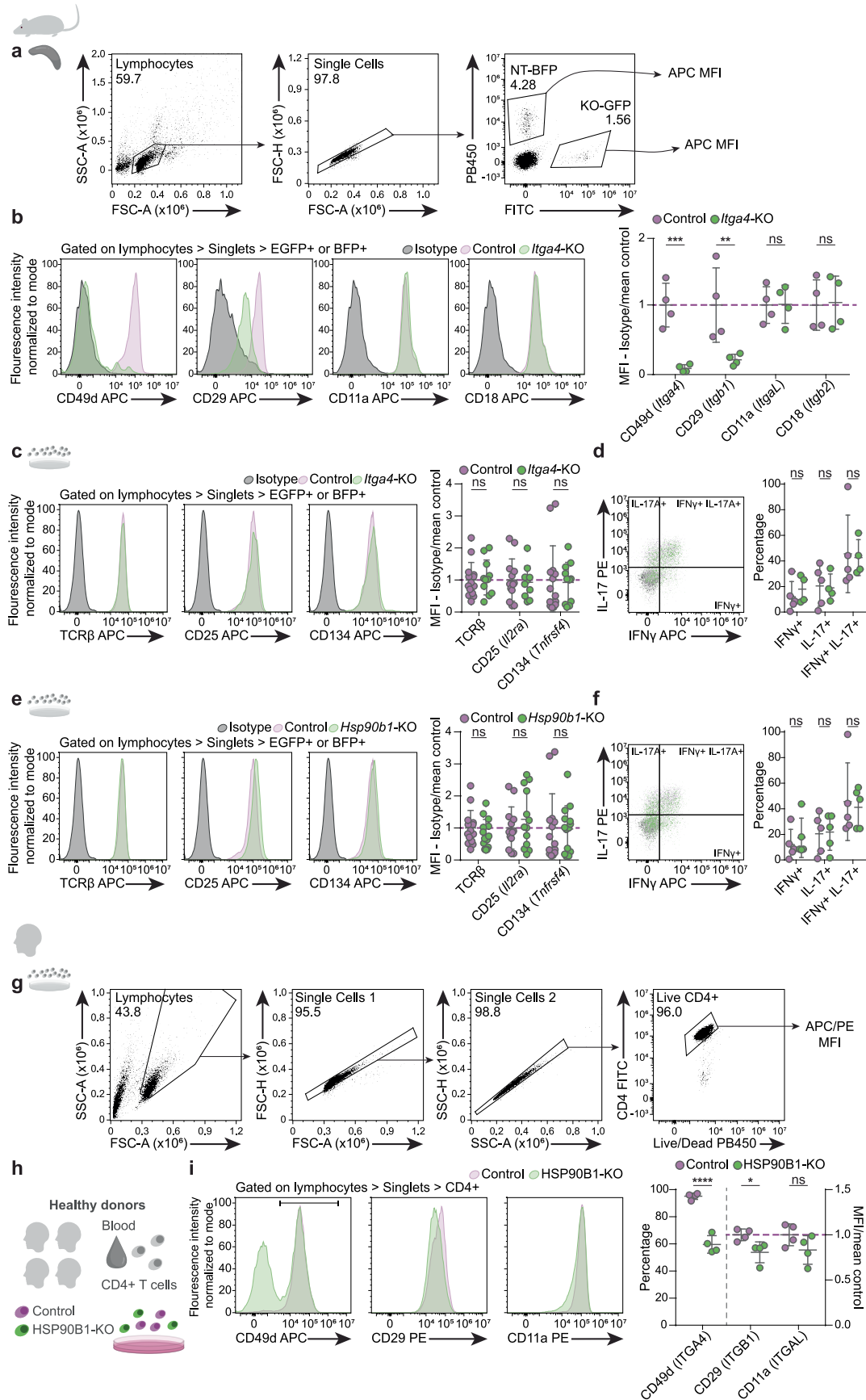
Extended Data Fig. 2 | miRNA based regulation of T cell migration to the CNS. a. Genome-wide screen results across different tissue compartments, comparing (from left to right) meninges or parenchyma to blood and meninges or parenchyma to spleen. Lines indicate $p\text{-value} = 0.05$ and $\text{log}_2(\text{Fold Change}) = \pm 0.5$. Green, miRNAs, lilac controls. b. Results from the

validation screen showing the miRNAs that were included, comparing (from top to bottom) meninges or parenchyma to blood and meninges or parenchyma to spleen. Star indicates $p\text{-value} < 0.05$, absolute $\text{log}_2(\text{Fold Change}) > 3$ standard deviations of the sample and ≥ 3 “neg/pos|goodsgrna”.



Extended Data Fig. 3 | Genes regulating differential migration between spinal cord parenchyma and meninges or between spleen and blood. a-d, Validation screen results showing the top-ranking genes whose KO showed impaired (a) or enhanced (c) migration of TMBP cells to the spinal cord parenchyma compared to the meninges, and b,d, $\text{log}_2(\text{Fold Change})$ heatmaps showing the genes essential for "facilitating" TMBP cell entry to the parenchyma compared to the meninges (KO impairs migration, blue) (b) or for "braking" migration to the parenchyma compared to meninges (KO enhances migration, red) (d).

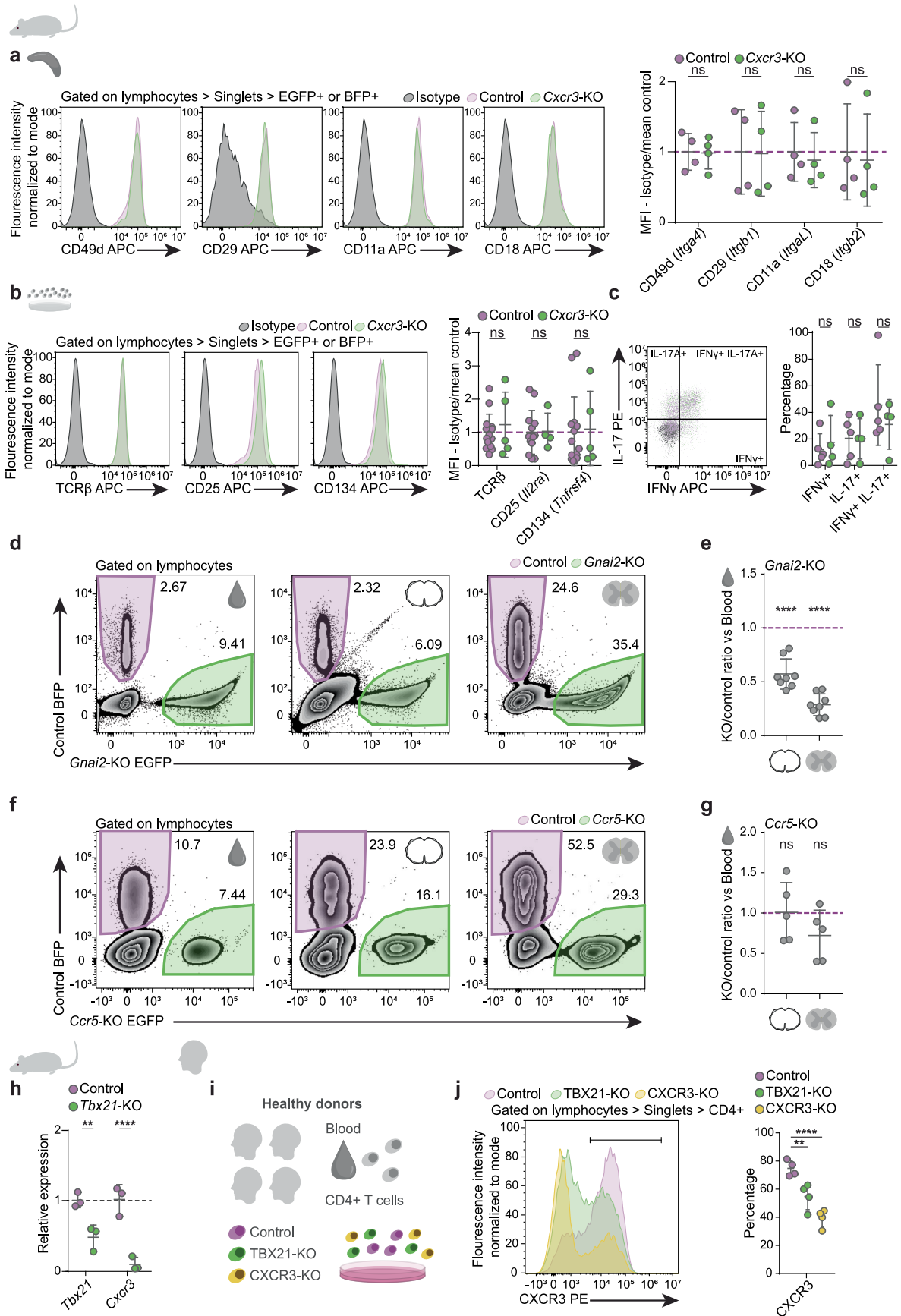
e-h, Validation screen results showing the top-ranking genes whose KO showed impaired (e) or enhanced (g) migration of TMBP cells to the spleen compared to blood, and f,h, $\text{log}_2(\text{Fold Change})$ heatmaps showing the genes essential for "facilitating" TMBP cell entry to the spleen from the blood (KO impairs migration, blue) (f) or for "braking" spleen migration (KO enhances migration, red) (h). Stars indicate, for all heatmaps, $p\text{-value} < 0.05$, absolute $\text{log}_2(\text{Fold Change}) > 3$ standard deviations of the $\text{log}_2(\text{Fold Change})$ of the controls and ≥ 3 "neg/pos|goodsgrna".



Extended Data Fig. 4 | See next page for caption.

Extended Data Fig. 4 | Effects of editing components of the adhesion module in rat TMBP cells and human CD4 + T cells. a, Gating strategy for rat T cell experiments. An example spleen sample is shown. b, Representative flow cytometry plots of integrin surface stainings of Itga4-KO and control TMBP cells isolated from the spleen of co-transferred rats 3 days post-transfer, grey isotype control, lilac control, green KO. Right, quantification of the MFI with isotype background subtraction normalized to the mean control intensity. n = 4 rats. c,e, Representative flow cytometry plots of activation marker surface stainings from TMBP cells (control and Itga4-KO (c) or Hsp90b1-KO (e)) in vitro at 2 days post restimulation; grey, isotype control; lilac, control; green, KO. Right, quantification of the MFI with isotype background subtraction normalized to the mean control intensity. n = 14 independent experiments for control and Hsp90b1-KO, TCR β and CD134; n = 13 control and Hsp90b1-KO, CD25; n = 11 Itga4-KO, TCR β and CD134; n = 10 Itga4-KO, CD25. d,f, Representative flow cytometry plots of intracellular cytokine staining from TMBP cells (control and Itga4-KO

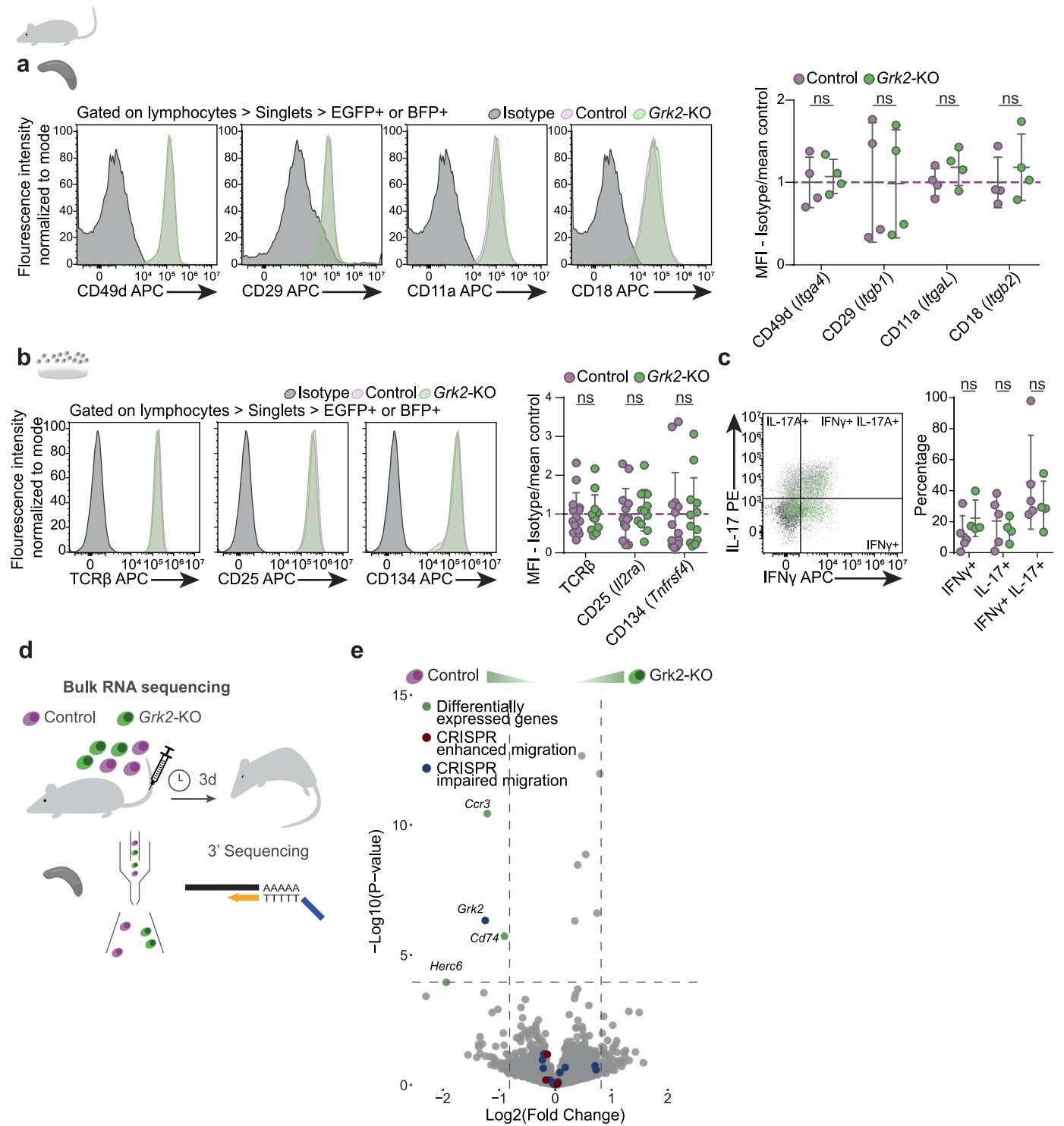
(d) or Hsp90b1-KO (f)) in vitro at 1 day post restimulation, grey isotype control, lilac control, green KO. Right, quantification of the percentages. n = 5 independent experiments for control and Hsp90b1-KO; n = 4 for Itga4-KO. g, Gating strategy for human T cell experiments. h, Experimental design of human HSP90B1-KO CD4 + T cell surface stainings. i, Representative flow cytometry plots of integrin surface stainings from in vitro HSP90B1-KO human CD4 + T cells; lilac, control, green, KO. Right, quantification of the percentage or of the MFI normalized to the mean control intensity. n = 4 donors. b-f,i MFI, two-way ANOVA (b, F = 13.37, P = 0.0013; c, F = 0.01785, P ns; d, F = 0.00591, P ns; e, F = 0.0119, P ns; f, F = 0.01325, P ns; i, F = 9.179, P = 0.0105) with multiple comparisons with the two-stage linear step-up procedure of Benjamini, Krieger and Yekutieli, i, percentage, unpaired t-test. Control FACS datapoints for in vitro surface (c,e) and intracellular stainings (d,f) are the same for all KOs, which were analysed in parallel (cf. Extended Data Figs. 5, 6 and 7). Figures show mean \pm s.d. P > 0.05 ns (non-significant), P < 0.05 *, P < 0.01 **, P < 0.001 ***, P < 0.0001 ****.



Extended Data Fig. 5 | See next page for caption.

Extended Data Fig. 5 | Effects of editing components of the chemotaxis module in rat TMBP cells and human CD4⁺ T cells. a, Representative flow cytometry plots of integrin surface stainings of Cxcr3-KO and control TMBP cells isolated from the spleen of co-transferred rats 3 days post-transfer; grey, isotype control; lilac, control; green, KO. Right, quantification of the MFI with isotype background subtraction normalized to the mean control intensity. $n = 4$ rats. b, Representative flow cytometry plots of activation marker surface stainings from TMBP cells (control and Cxcr3-KO) in vitro at 2 days post restimulation; grey, isotype control; lilac, control; green, KO. Right, quantification of the MFI with isotype background subtraction normalized to the mean control intensity. $n = 14$ independent experiments for control TCR β and CD134; $n = 13$ control for CD25; $n = 5$ for Cxcr3-KO, TCR β and CD134; $n = 4$ for Cxcr3-KO, CD25. c, Representative flow cytometry plots of intracellular cytokine staining from TMBP cells (control and Cxcr3-KO) in vitro at 1 day post restimulation; grey, isotype control; lilac, control; green, KO. Right, quantification of the percentages. $n = 5$ independent experiments for control; $n = 4$ for Cxcr3-KO. d,f, Representative flow cytometry plots of T cells from blood, meninges and parenchyma after a co-transfer experiment with control and Gnai2-KO (d) or Ccr5-KO (f) TMBP cells.

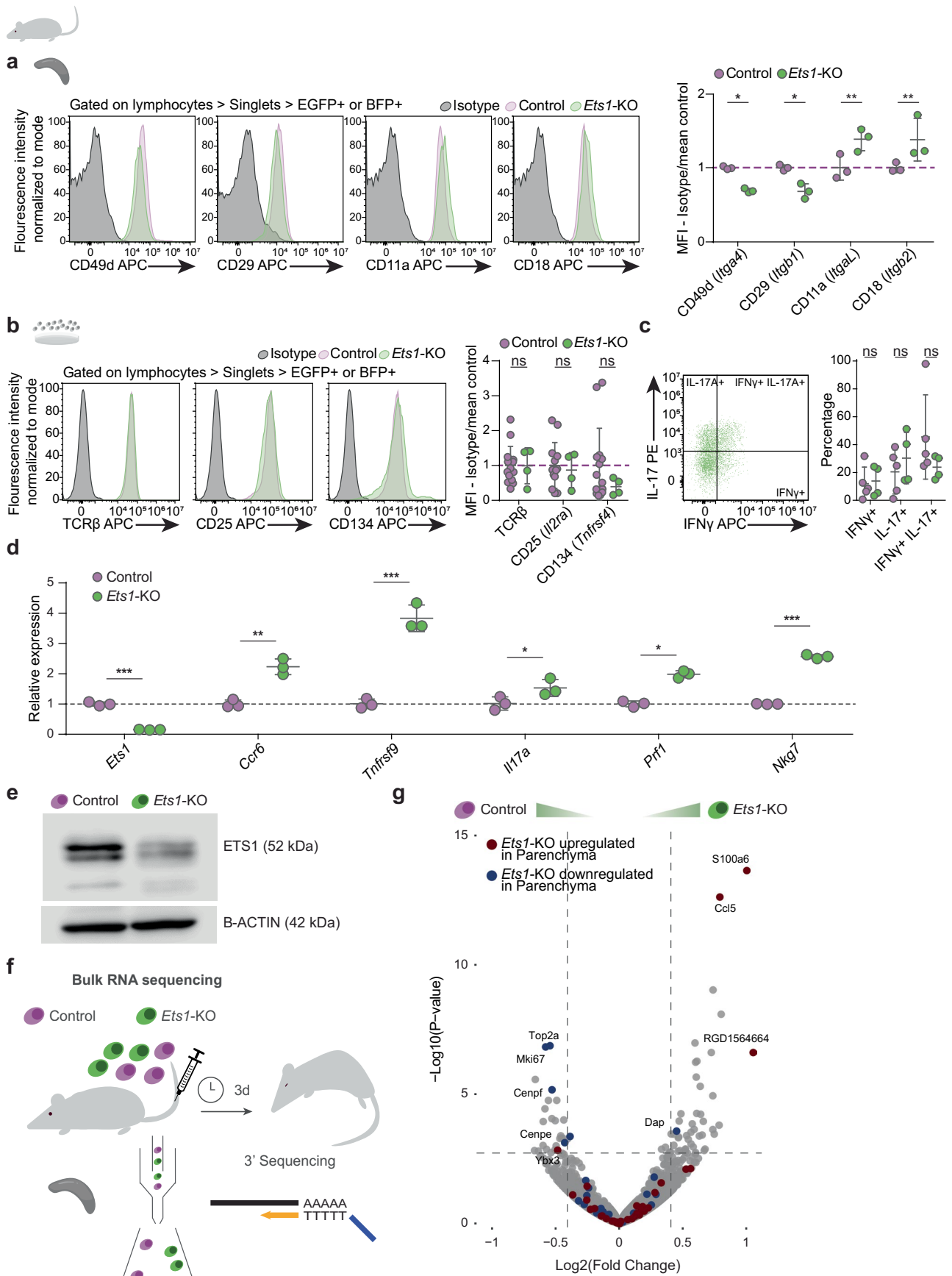
e.g, Migratory phenotype of Gnai2-KO (e) or Ccr5-KO (g) cells compared to control, shown as the ratio of KO/control in meninges (left) or parenchyma (right) normalized to the KO/control ratio in blood. $n = 8$ rats for Gnai2-KO, $n = 5$ for Ccr5-KO. h, qPCR results in Tbx21-KO and control cells in vitro. $n = 3$ samples per group. i, Experimental design of human TBX21-KO and CXCR3-KO control T cell surface stainings. j, Representative flow cytometry plots of control and KO cells stained for CXCR3. Right, quantification of the percentage. $n = 4$ donors. a,b,c, ordinary two-way ANOVA (a, $F = 0.1481$, P ns; b, $F = 0.2169$, P ns; c, $F = 0.172$, P ns) with multiple comparisons with the two-stage linear step-up procedure of Benjamini, Krieger and Yekutieli. e.g, one sample t-test against hypothetical mean = 1. h, multiple paired t-tests with two-stage linear step-up procedure of Benjamini, Krieger and Yekutieli multiple testing correction. j, ordinary one-way ANOVA ($F = 23.96$, $P = 0.0002$) with multiple comparisons with the two-stage linear step-up procedure of Benjamini, Krieger and Yekutieli. Control FACS datapoints for in vitro surface (b) and intracellular stainings (c) are the same for all KOs, which were analysed in parallel (cf. Extended Data Figs. 4, 6 and 7). Figures show mean \pm s.d., $P > 0.05$ ns (non-significant), $P < 0.05$ *, $P < 0.01$ ***, $P < 0.001$ ***, $P < 0.0001$ ****.



Extended Data Fig. 6 | See next page for caption.

Extended Data Fig. 6 | Effects of editing Grk2 on adhesion, activation, cytokine production and transcriptional profile of rat TMBP cells. a, Representative flow cytometry plots of integrin surface stainings of Grk2-KO and control TMBP cells isolated from the spleen of co-transferred rats 3 days post-transfer; grey, isotype control; lilac, control; green, KO. Right, quantification of the MFI with isotype background subtraction normalized to the mean control intensity. $n = 4$ rats. b, Representative flow cytometry plots of activation marker surface stainings from TMBP cells (control and Grk2-KO) in vitro at 2 days post restimulation; grey, isotype control; lilac, control; green, KO. Right, quantification of the MFI with isotype background subtraction normalized to the mean control intensity. $n = 14$ independent experiments for control TCR β and CD134; $n = 13$ for control, CD25; $n = 12$ for Grk2-KO, TCR β and CD134; $n = 11$ for Grk2-KO, CD25. c, Representative flow cytometry plots of intracellular cytokine staining from TMBP cells (control and Grk2-KO) in vitro at 1 day post restimulation; grey, isotype control; lilac, control; green, KO. Right,

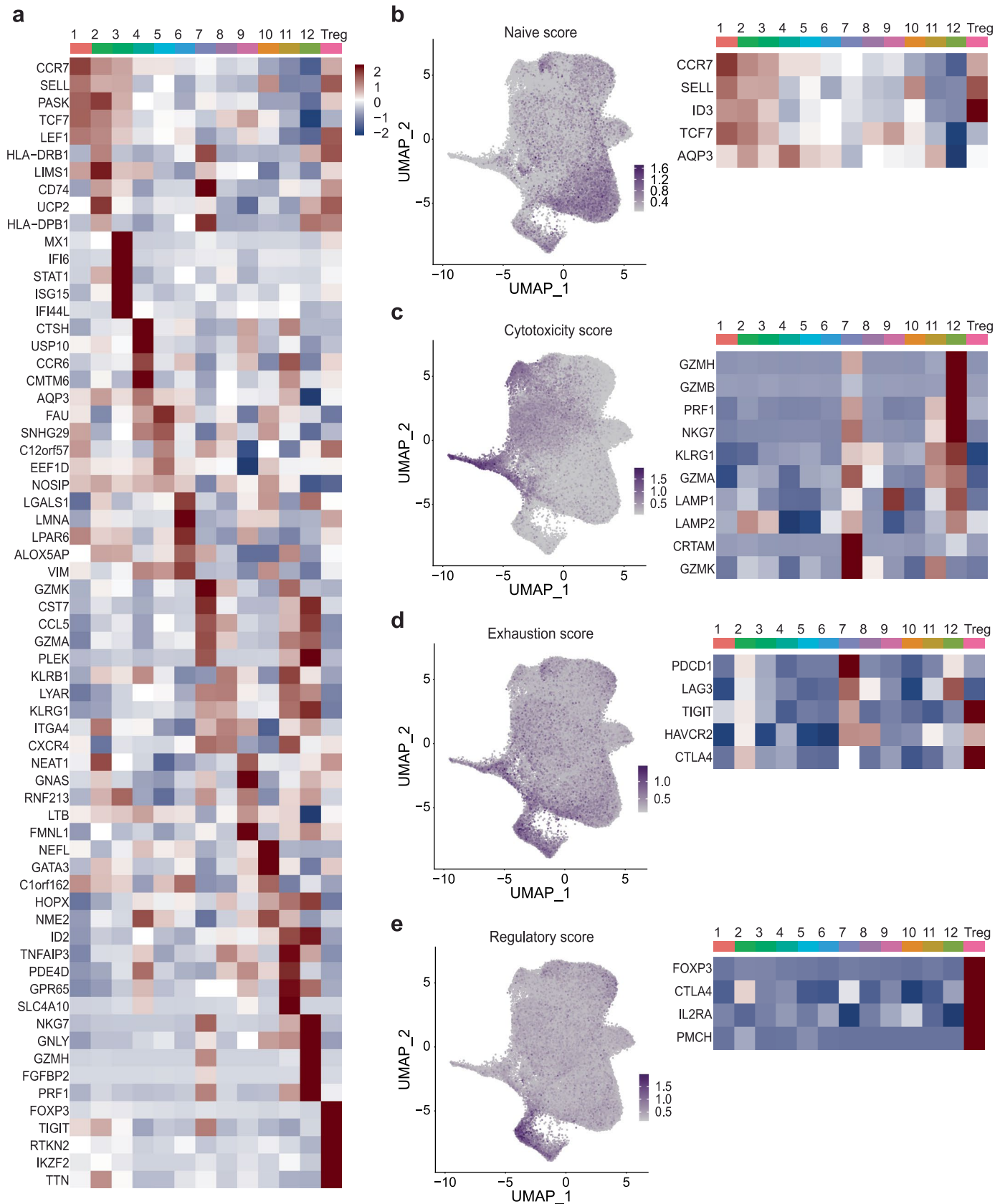
quantification of the percentages. $n = 5$ independent experiments for control; $n = 4$ for Grk2-KO. d, Experimental design of the bulk RNAseq experiment of Grk2-KO and control TMBP cells from the spleen of co-transferred animals. e, Volcano plot of the RNAseq results of Grk2-KO cells compared to control TMBP cells, lines indicate adjusted p -value = 0.05 and $\log_2(\text{Fold Change}) = \pm 3$ standard deviations of the sample. Green, significantly differentially expressed genes; blue, essential genes "facilitating" CNS migration in TMBP cells ("CRISPR impaired migration"); red, essential genes "braking" CNS migration ("CRISPR enhanced migration") from Fig. 1d,f. Control FACS datapoints for in vitro surface (b) and intracellular stainings (c) are the same for all KOs, which were analysed in parallel (cf. Extended Data Figs. 4, 5 and 7). a,b,c, two-way ANOVA (a, $F = 0.5042$, P ns; b, $F = 0.06375$, P ns; c, $F = 0.2459$, P ns) with multiple comparisons with the two-stage linear step-up procedure of Benjamini, Krieger and Yekutieli. Figures show mean \pm s.d., $P > 0.05$ ns (non-significant), $P < 0.05$ *, $P < 0.01$ **, $P < 0.001$ ***, $P < 0.0001$ ****.



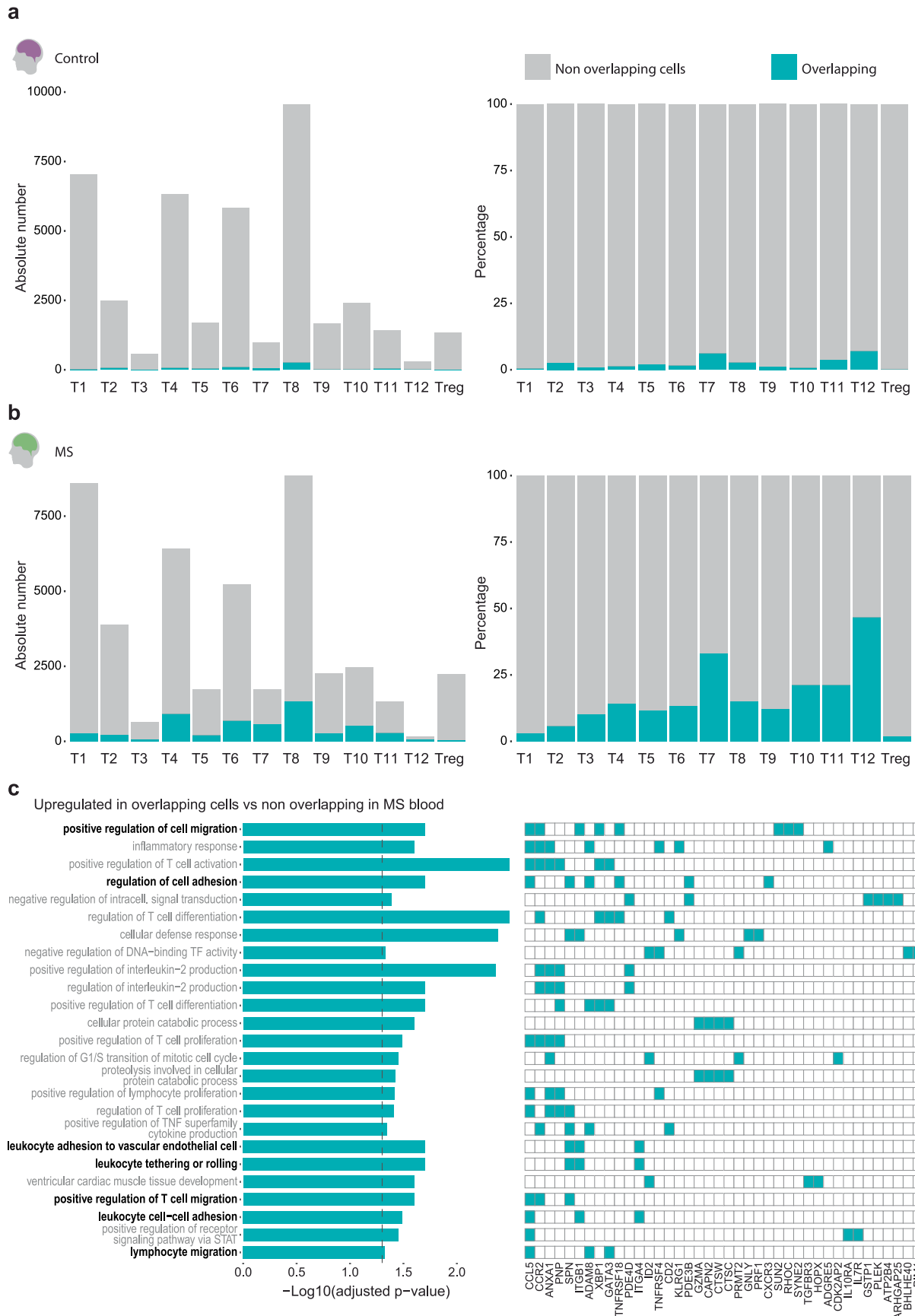
Extended Data Fig. 7 | See next page for caption.

Extended Data Fig. 7 | Effects of editing Ets1 on adhesion, activation, cytokine production and transcriptional profile of rat TMBP cells. a, Representative flow cytometry plots of integrin surface stainings of Ets1-KO and control TMBP cells isolated from the spleen of co-transferred rats 3 days post-transfer; grey, isotype control; lilac, control; green, KO. Right, quantification of the MFI with isotype background subtraction normalized to the mean control intensity. $n = 3$ rats. b, Representative flow cytometry plots of activation marker surface stainings from TMBP cells (control and Ets1-KO) in vitro at 2 days post restimulation; grey, isotype control; lilac, control; green, KO. Right, quantification of the MFI with isotype background subtraction normalized to the mean control intensity. $n = 14$ independent experiments for control, TCR β and CD134; $n = 13$ for control, CD25; $n = 4$ for Ets1-KO. c, Representative flow cytometry plots of intracellular cytokine staining from TMBP cells (control and Ets1-KO) in vitro at 1 day post restimulation; grey, isotype control; lilac, control; green, KO. Right, quantification of the percentages. $n = 5$ independent experiments for control; $n = 4$ Ets1-KO. d, qPCR validation of selected upregulated genes in the Ets1-KO cells driving the upregulated pathways. $n = 3$ samples per

group. e, Western blot showing the downregulation of ETS1 protein levels in the KO cells. $n = 1$. f, Experimental design of the bulk RNAseq experiment of Ets1-KO and control TMBP cells from the spleen of co-transferred animals. g, Volcano plot of the RNAseq results of Ets1-KO cells compared to control TMBP cells in the spleen, lines indicate adjusted p -value = 0.05 and $\log_2(\text{Fold Change}) = \pm 3$ standard deviations of the sample. Blue, genes downregulated in the Ets1-KO compared to control in parenchyma ("Ets1-KO downregulated in parenchyma"); red, genes upregulated in the Ets1-KO compared to control in parenchyma ("Ets1-KO upregulated in parenchyma"). Control FACS datapoints for in vitro surface (b) and intracellular stainings (c) are the same for all KOs, which were analysed in parallel (cf. Extended Data Figs. 4, 5 and 6). a,b,c, two-way ANOVA (a, $F = 0.3755$, P ns; b, $F = 1.066$, P ns; c, $F = 0.2231$, P ns) with multiple comparisons with the two-stage linear step-up procedure of Benjamini, Krieger and Yekutieli. d, multiple paired t-tests with two-stage linear step-up procedure of Benjamini, Krieger and Yekutieli multiple testing correction. Figures show mean \pm s.d, $P > 0.05$ ns (non-significant), $P < 0.05$ *, $P < 0.01$ **, $P < 0.001$ ***, $P < 0.0001$ ****.



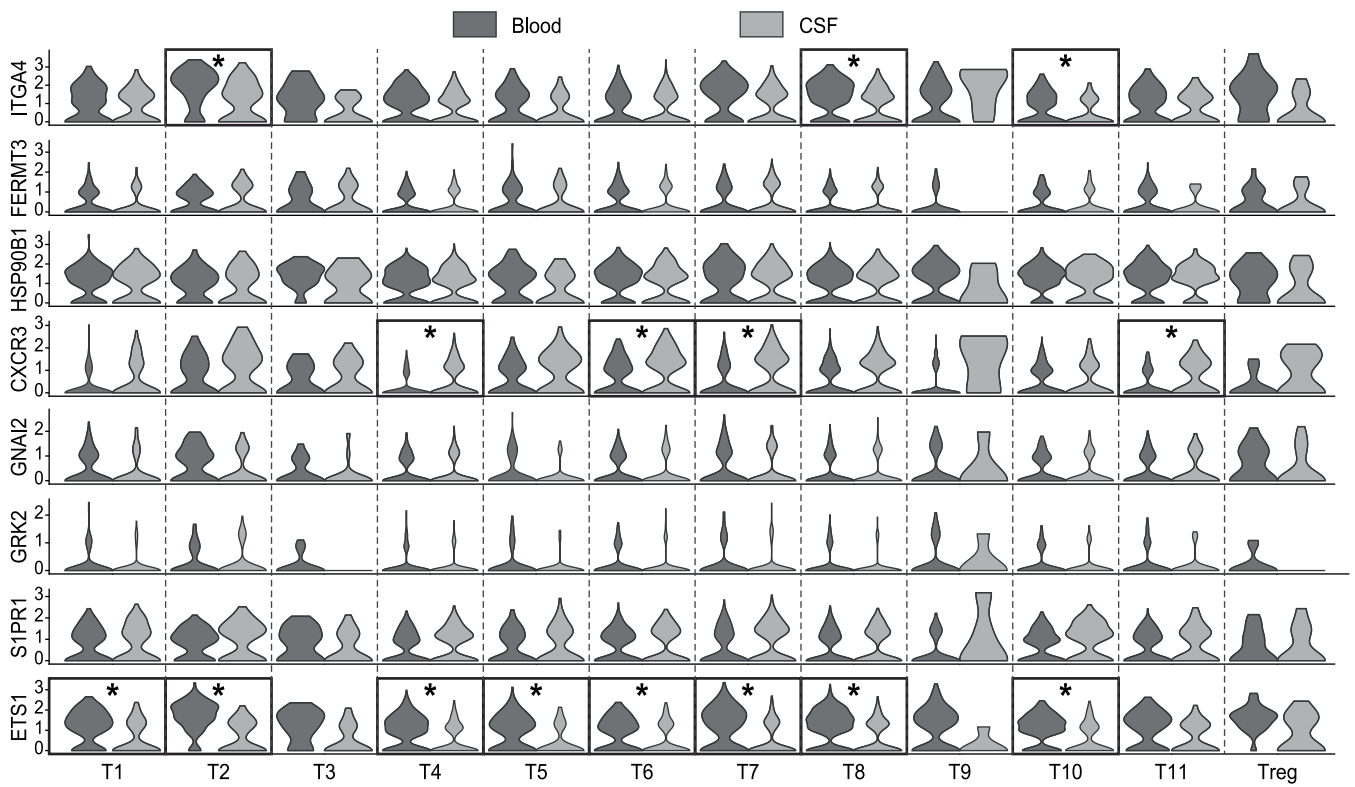
Extended Data Fig. 8 | Molecular characterization of CD4⁺ T cell clusters. a, Heatmap showing the relative expression levels of the top five differentially regulated genes per cluster. b-e, Naïve (b), cytotoxicity (c), exhaustion (d) and regulatory (e) T cell marker gene expression, across cells (left) and clusters (right).



Extended Data Fig. 9 | See next page for caption.

Extended Data Fig. 9 | Differentially regulated pathways in T cell clones overlapping between CSF and blood in patients with MS. a, b, Absolute (left) and relative (right) numbers of overlapping CD4 + T cells (defined as cells belonging to a clone whose TCR was found in blood and CSF cells of the same donor) across clusters in controls (a) and in patients with MS (b). c, Pathway

analysis of the top upregulated pathways in overlapping CD4 + T cells in the blood of patients with MS compared to non overlapping cells in the same compartment, left panel shows differentially regulated pathways and right panel shows the top differential regulated genes in these pathways. In bold, pathways related to migration.



Extended Data Fig. 10 | Expression pattern of essential regulators in human CD4 + T cells from blood and CSF. Violin plots comparing selected gene expression levels between T cells (analysed per cluster) from blood (dark grey) and CSF (light grey) in patients with MS for those CD4 + T cell clones whose

TCR sequences were detected in blood and CSF. Stars indicate significance as per adjusted $P < 0.05$ and absolute $\log_2(\text{Fold Change}) > 3$ times the standard deviation of the sample. Stars indicate adjusted p-value < 0.05 when comparing MS CSF to blood.

Reporting Summary

Nature Portfolio wishes to improve the reproducibility of the work that we publish. This form provides structure for consistency and transparency in reporting. For further information on Nature Portfolio policies, see our [Editorial Policies](#) and the [Editorial Policy Checklist](#).

Statistics

For all statistical analyses, confirm that the following items are present in the figure legend, table legend, main text, or Methods section.

n/a Confirmed

- The exact sample size (n) for each experimental group/condition, given as a discrete number and unit of measurement
- A statement on whether measurements were taken from distinct samples or whether the same sample was measured repeatedly
- The statistical test(s) used AND whether they are one- or two-sided
Only common tests should be described solely by name; describe more complex techniques in the Methods section.
- A description of all covariates tested
- A description of any assumptions or corrections, such as tests of normality and adjustment for multiple comparisons
- A full description of the statistical parameters including central tendency (e.g. means) or other basic estimates (e.g. regression coefficient) AND variation (e.g. standard deviation) or associated estimates of uncertainty (e.g. confidence intervals)
- For null hypothesis testing, the test statistic (e.g. F , t , r) with confidence intervals, effect sizes, degrees of freedom and P value noted
Give P values as exact values whenever suitable.
- For Bayesian analysis, information on the choice of priors and Markov chain Monte Carlo settings
- For hierarchical and complex designs, identification of the appropriate level for tests and full reporting of outcomes
- Estimates of effect sizes (e.g. Cohen's d , Pearson's r), indicating how they were calculated

Our web collection on [statistics for biologists](#) contains articles on many of the points above.

Software and code

Policy information about [availability of computer code](#)

Data collection Galaxy platform (Je-Demultiplex-Illu (Galaxy Version 1.2.1), Cutadapt (Galaxy Version 4.4+galaxy0), Trimmomatic (Galaxy Version 0.39+galaxy0)), FACS Suite 1.06 (FACS VERSE), FACSDiva 8.0 (BD FACS Aria Fusion, FACS Fortessa), CytExpert 2.5.0.77 (Cytoflex S), Image Studio Lite Software version 5.2 (Odyssey FC, OFC-0661), Bio-Rad CFX Maestro 1.1 version 4.1.2433.1219 (Bio-Rad CFX Connect Real-Time PCR system), ICE software tool (version 2.0+)

Data analysis MAGeCK (version 0.5.7.1+), R (version 4.0.0+), tidyverse, Seurat v.4.1.0, MAST v.1.16.0, enrichR (v3.1), Cell ranger 10X Genomics v.6.1, Fiji (version 1.53e), RNA STAR (version 2.7.2b), HTSeq-count (version 1.0.0), DESeq2 (version 2.11.40.7+galaxy1), gProfiler (version of 2019), FlowJO (version 10+), GraphPad Prism (version 7+), Excel (Microsoft Office, 2016+)
Custom code used for the analysis of the data for this paper are uploaded as supplementary code in the supplementary information.

For manuscripts utilizing custom algorithms or software that are central to the research but not yet described in published literature, software must be made available to editors and reviewers. We strongly encourage code deposition in a community repository (e.g. GitHub). See the Nature Portfolio [guidelines for submitting code & software](#) for further information.

Data

Policy information about [availability of data](#)

All manuscripts must include a [data availability statement](#). This statement should provide the following information, where applicable:

- Accession codes, unique identifiers, or web links for publicly available datasets
- A description of any restrictions on data availability
- For clinical datasets or third party data, please ensure that the statement adheres to our [policy](#)

Next-generation sequencing raw data and processed gene expression data that support the findings of this study are deposited into GEO under the accession

Field-specific reporting

Please select the one below that is the best fit for your research. If you are not sure, read the appropriate sections before making your selection.

- Life sciences Behavioural & social sciences Ecological, evolutionary & environmental sciences

For a reference copy of the document with all sections, see [nature.com/documents/nr-reporting-summary-flat.pdf](https://www.nature.com/documents/nr-reporting-summary-flat.pdf)

Life sciences study design

All studies must disclose on these points even when the disclosure is negative.

Sample size	For the CRISPR screens, the sample size was determined based on the number of cells needed to maintain a minimum of 100x and a maximum of 1,000x coverage in all relevant cell populations, with the aim to minimize false discovery rates and ensure statistically meaningful data, while also considering the practicality of handling the required number of cells. Replicate number was chosen based on Ong et al, Scientific Reports 2017. No statistical methods were used to pre-determine sample sizes but our sample sizes are similar to those reported in previous publications (See Ref. Odoardi et al., Nature 2012, Bartholomäus et al., Nature 2009, Schläger et al., Nature 2016, Kawakami et al., Journal of Experimental Medicine 2004). For the analysis of human CD4+ T cells by NGS, the samples from MS and control patients were selected due to availability of sufficient biomaterials.
Data exclusions	For in vivo migration assay (co-transfer experiments, Fig. 2c,g; 3b; 4b,i; 6b; Extended Data Fig. 5e,g), FACS data samples from the whole animal were excluded when <100 individual cells were detected in any population of interest.
Replication	All animal experiments in this study include at least three independent biological replicates. The number of replicates is mentioned in the corresponding figure legend of each experiment. All replicated experiments were successful, except when prior exclusion criteria were met. 15,768 and 807 CSF derived and 29,749 and 40,845 blood derived CD4+ T cells from 4 MS patients and 4 control patients were used for NGS, respectively
Randomization	Rats were randomly allocated into experimental groups. Human samples were allocated by MS patients and control patients. The samples were not randomized.
Blinding	Investigators were not blinded during experiments due to the nature of the binary type of experiments (e.g. co-transfer experiments: BFP vs GFP labeled cell, disease course: obvious disease phenotype control vs EAE). The analysis of NGS data is unbiased. Therefore, investigators were not blinded.

Reporting for specific materials, systems and methods

We require information from authors about some types of materials, experimental systems and methods used in many studies. Here, indicate whether each material, system or method listed is relevant to your study. If you are not sure if a list item applies to your research, read the appropriate section before selecting a response.

Materials & experimental systems

n/a	Included in the study
<input type="checkbox"/>	<input checked="" type="checkbox"/> Antibodies
<input type="checkbox"/>	<input checked="" type="checkbox"/> Eukaryotic cell lines
<input checked="" type="checkbox"/>	<input type="checkbox"/> Palaeontology and archaeology
<input type="checkbox"/>	<input checked="" type="checkbox"/> Animals and other organisms
<input type="checkbox"/>	<input checked="" type="checkbox"/> Human research participants
<input checked="" type="checkbox"/>	<input type="checkbox"/> Clinical data
<input checked="" type="checkbox"/>	<input type="checkbox"/> Dual use research of concern

Methods

n/a	Included in the study
<input checked="" type="checkbox"/>	<input type="checkbox"/> ChIP-seq
<input type="checkbox"/>	<input checked="" type="checkbox"/> Flow cytometry
<input checked="" type="checkbox"/>	<input type="checkbox"/> MRI-based neuroimaging

Antibodies

Antibodies used

unconjugated mouse IgG1 Isotype control (Sigma, Cat#: M-1398, clone MOPC31c, Lot#: 084K4862, dilution: 1:100), unconjugated NA/LE armenian hamster IgG2 Isotype control (BD Pharmingen, Cat#: 553961, clone Ha4/8, Lot#: 5105640, dilution: 1:100), rat IgG1 Isotype control-PE (BD Pharmingen, Cat#: 554685, clone R3-34, Lot#: 87970, dilution: 1:100), unconjugated mouse anti-rat CD49d (Thermo Fisher, Cat#: MA49D7, clone TA-2, Lot#: WG334936, dilution: 1:100), unconjugated mouse anti-rat CD11a (Biolegend, Cat#: 201902, clone wt.1, Lot#: B267211, dilution: 1:100),

unconjugated mouse anti-rat CD18 (Thermo Fisher, Cat#: MA1817, clone wt.3, Lot#: RK245842, dilution: 1:100), unconjugated mouse anti-rat TCRbeta (BD Pharmingen, Cat#: 554911, clone R73, Lot#: 0199116, dilution: 1:100), unconjugated mouse anti-rat CD25 (Thermo Fisher, Cat#: MA517490, clone OX39, Lot#: VJ3104933, dilution: 1:100), unconjugated mouse anti-rat CD134 (Thermo Fisher, Cat#: MA1-70020, clone OX40, Lot#: YC3847111, dilution: 1:100), unconjugated armenian hamster anti-rat CD29 (Biolegend, Cat#: 102202, clone HMβ1-1, Lot#: B326869, dilution: 1:100), rat anti-mouse/rat IL-17A-PE (BD Pharmingen, Cat#: 559502, clone TC11-18H10, Lot#: 81990, dilution: 1:100), unconjugated mouse anti-rat IFNγ (eBioscience, Cat#: 14-7310-85, clone DB1, Lot#: E05481-500, dilution: 1:100), donkey anti-mouse IgG-APC (Jackson ImmunoResearch, Cat#: 715-136-151, polyclonal, Lot#: 122609, dilution: 1:1000), goat anti-armenian hamster IgG-APC (Jackson ImmunoResearch, Cat#: 127-135-160, polyclonal, Lot#: 150828, dilution: 1:1000), goat anti-mouse IgG-AF647 (SouthernBiotech, Cat#1038-31, polyclonal, Lot#: C1717-N190C, dilution: 1:1000), mouse anti-human-CD4-FITC (Biolegend, Cat#: 344604, clone SK3, Lot#: B331829, dilution: 1:100), mouse anti-human-S1PR1-eF660 (Thermo Fisher, Cat#: 50-3639-41, clone SW4GYPP, Lot#: 2349796, dilution: 1:100), mouse anti-human CD45RO-FITC (Thermo Fisher, Cat#: 11-0457-42, clone UCHL1, Lot#: 4272459, dilution: 1:40), rat anti-human CCR7-APC (Thermo Fisher, Cat#: 17-1979-42, clone 3D12, Lot#: 4290631, dilution: 1:40), mouse anti-human CD3-AF700 (Thermo Fisher, Cat#: 56-0037-42, clone OKT3, Lot#: 4330031, dilution: 1:50), mouse anti-human CD4-Pacific Blue (Thermo Fisher, Cat#: MHCD0428, clone S3.5, Lot#: 2123513, dilution: 1:25), mouse anti-human CD8-PerCP (BioLegend, Cat#: 344708, clone SK1, Lot#: B204989, dilution: 1:25), rabbit anti-rat ETS1 (Cell Signaling Technology, Cat#: 14069S, clone D808A, Lot #: 3, dilution: 1:1000), mouse anti-beta Actin Antibody HRP (Santa Cruz, Cat#: sc-47778 HRP, clone C4, Lot #: A2418, dilution: 1:100000), mouse anti-rabbit IgG-HRP (Santa Cruz, Cat#: sc-2357 HRP, secondary antibody, Lot #: A0318, dilution: 1:10000), rabbit anti-GRK2 (Cell Signaling Technology, Cat#: 74761S, polyclonal, Lot #: 1, dilution: 1:1000), rabbit anti-Phospho-p44/42 MAPK(Erk1/2)(Thr202/Tyr204) (Cell Signaling Technology, Cat#: 4370T, clone D13.14.4E, Lot #: 28, dilution: 1:1000),

rabbit anti-p44/42 MAPK(Erk1/2) (Cell Signaling Technology, Cat#: 4695T, clone 137F5, Lot #: 35, dilution: 1:1000), anti-human-CD49d-APC (Biolegend, Cat#: 304307, clone 9F10, Lot#: B270194, dilution: 1:100), anti-human CXCR3-PE (Biolegend, Cat#: 353705, clone G025H7, Lot#: B342049, dilution: 1:100), anti-human CD29-PE (Biolegend, Cat#: 303003, clone TS2/16, Lot#: B358184, dilution: 1:100), anti-human CD11a-PE (Biolegend, Cat#: 301207, clone HI111, Lot#: B319403, dilution: 1:100), mouse anti-human CD3 (Thermo Fisher, Cat#: 16-0037-81, clone OKT3, Lot#: 2493171), mouse anti-human CD28 (Thermo Fisher, Cat#: 16-0289-81, clone CD28.2, Lot#: 2470259) anti-human CD4 (Catalog no: 300567; Lot no: B300113; Clone: RPA-T4) anti-human CD8a (Catalog no: 301071; Lot no: B315106; Clone: RPA-T8) isotype mlgG1-control-Ab (Catalog no: 400187; Lot no: B333559; Clone: MOPC-21)

Validation

Antibodies were commercially available and validated by the manufacturers or used in previous studies according to manufactures:

Flow cytometry:

unconjugated mouse IgG1 Isotype control (Sigma, Cat#: M-1398) : 8 citations
 unconjugated NA/LE armenian hamster IgG2 Isotype control (BD Pharmingen, Cat#: 553961) : 4 citations
 rat IgG1 Isotype control-PE (BD Pharmingen, Cat#: 554685) : data sheet
 unconjugated mouse anti-rat CD49d (Thermo Fisher, Cat#: MA49D7) : data sheet
 unconjugated mouse anti-rat CD11a (Biolegend, Cat#: 201902) : data sheet
 unconjugated mouse anti-rat CD18 (Thermo Fisher, Cat#: MA1817) : data sheet
 unconjugated mouse anti-rat TCRbeta (BD Pharmingen, Cat#: 554911) : data sheet
 unconjugated mouse anti-rat CD25 (ThermoFisher, Cat#: MA517490) : data sheet
 unconjugated mouse anti-rat CD134 (Invitrogen, Cat#: MA1-70020) : data sheet
 unconjugated armenian hamster anti-rat CD29 (Biolegend, Cat#: 102202) : data sheet
 rat anti-mouse IL-17A-PE (BD Pharmingen, Cat#: 559502) : data sheet
 unconjugated mouse anti-rat IFNγ (eBioscience, Cat#: 14-7310-85) : 38 citations
 mouse anti-human-CD4-FITC (Biolegend, Cat#: 344604) : data sheet
 mouse anti-human-S1PR1-eF660 (Thermo Fisher, Cat#: 50-3639-41) : data sheet
 mouse anti-human CD45RO-FITC (Thermo Fisher, Cat#: 11-0457-42) : data sheet
 rat anti-human CCR7-APC (Thermo Fisher, Cat#: 17-1979-42) : data sheet
 mouse anti-human CD3-AF700 (Thermo Fisher, Cat#: 56-0037-42) : data sheet
 mouse anti-human CD4-Pacific Blue (Thermo Fisher, Cat#: MHCD0428) : data sheet
 mouse anti-human CD8-PerCP (BioLegend, Cat#: 344708) : data sheet
 mouse anti-human-CD49d-APC (Biolegend, Cat#: 304307) : data sheet
 mouse anti-human CXCR3-PE (Biolegend, Cat#: 353705) : data sheet
 mouse anti-human CD29-PE (Biolegend, Cat#: 303003) : data sheet
 mouse anti-human CD11a-PE (Biolegend, Cat#: 301207) : data sheet
 Westernblot:
 rabbit anti-rat ETS1 (Cell Signaling Technology, Cat#: 14069S) : data sheet
 mouse anti-beta Actin Antibody HRP (Santa Cruz, Cat#: sc-47778 HRP) : data sheet
 rabbit anti-GRK2 (Cell Signaling Technology, Cat#: 74761S) : data sheet
 rabbit anti-Phospho-p44/42 MAPK(Erk1/2)(Thr202/Tyr204) (Cell Signaling Technology, Cat#: 4370T) : data sheet
 rabbit anti-p44/42 MAPK(Erk1/2) (Cell Signaling Technology, Cat#: 4695T) : data sheet

Functional assay:

mouse anti-human CD3 (Thermo Fisher, Cat#: 16-0037-81): 95 citations
 mouse anti-human CD28 (Thermo Fisher, Cat#: 16-0289-81): 32 citations
 scRNAseq:
 anti-human CD4 (Catalog no: 300567; Lot no: B300113; Clone: RPA-T4): 8 citations
 anti-human CD8a (Catalog no: 301071; Lot no: B315106; Clone: RPA-T8): 2 citations
 isotype mlgG1-control-Ab (Catalog no: 400187; Lot no: B333559; Clone: MOPC-21): 3 citations

Eukaryotic cell lines

Policy information about [cell lines](#)

Cell line source(s)	HEK293 T cells (ATCC) GP+E86 (ATCC)
Authentication	Cell line was not authenticated after purchase
Mycoplasma contamination	Cell line was not tested for mycoplasma contamination but no indication of contamination was observed
Commonly misidentified lines (See ICLAC register)	No commonly misidentified cell lines were used.

Animals and other organisms

Policy information about [studies involving animals](#); [ARRIVE guidelines](#) recommended for reporting animal research

Laboratory animals	Lewis rats (LEW/Crl and LEW/OrlRj) were obtained from Charles River and Janvier. They were bred at the animal facility of Biomedical center, LMU. Both male and female rats at age between 5-20 weeks were used
Wild animals	The study did not involve wild animals.
Field-collected samples	The study did not involve samples collected from the field.
Ethics oversight	Regierung von Oberbayern

Note that full information on the approval of the study protocol must also be provided in the manuscript.

Human research participants

Policy information about [studies involving human research participants](#)

Population characteristics	Subjects in the MS group had been diagnosed with relapsing-remitting MS according to the revised McDonald criteria and had a relapse no longer than 45 days prior to lumbar puncture. All patients are female and age 27, 31, 32 and 41. Samples from four sex- and age (25, 25, 27 and 52)- matched individuals diagnosed with idiopathic intracranial hypertension were included in the control group. PBMCs of four healthy donors used for CRISPR gene editing were derived from leukoreduction system chambers.
Recruitment	<p>Patients with MS recruited for this study were seen at our outpatient department of the Institute of Clinical Neuroimmunology for clinical diagnostic work-up and CSF sampling was performed due to diagnostic purposes only. To reduce heterogeneity as well as confounders based on disease-modifying treatment, the RRMS-CSF cohort is composed of treatment naive patients with early MS only and only those patients were eligible for our study. Hence with regard to patient selection we can exclude any self-selection bias or other biases and the selection of patients has to the best of our knowledge no impact on the results. As non-inflammatory controls we obtained and analysed CSF samples from patients with idiopathic intracranial hypertension. In these cases lumbar puncture was performed as a therapeutic intervention only.</p> <p>We hereby confirm that all MS patients and controls (patients with IHH) included in the study have given a written informed consent. Recruitment of individuals took place from August 2020 to January 2021</p>
Ethics oversight	Written informed consent was obtained from all subjects according to the Declaration of Helsinki, Collection of samples was approved by local ethics committees of the LMU, Munich, ethical vote: 163-16 and LMU #18-821

Note that full information on the approval of the study protocol must also be provided in the manuscript.

Flow Cytometry

Plots

Confirm that:

- The axis labels state the marker and fluorochrome used (e.g. CD4-FITC).
- The axis scales are clearly visible. Include numbers along axes only for bottom left plot of group (a 'group' is an analysis of identical markers).
- All plots are contour plots with outliers or pseudocolor plots.
- A numerical value for number of cells or percentage (with statistics) is provided.

Methodology

Sample preparation	Blood was withdrawn by heart puncture into a heparinized syringe. Spleen, parathymic lymph nodes, and leptomeninges and parenchyma of the spinal cord were dissected and homogenized by passing through a metal strainer. Lymphocytes were
--------------------	--

isolated from blood by a Nycoprep gradient. First, the blood was diluted with an equal volume of PBS and overlaid onto Nycoprep. After centrifugation at 800 g, room temperature for 30 min with mild acceleration and brake, lymphocytes were collected from the interface. For spleen, erythrocytes were removed by treating with ACK buffer for 3 min on ice and lymphocytes were isolated using the EasySep™ Rat CD4+ T Cell Isolation Kit (StemCell, 19642), before purification by sorting. From the spinal cord parenchyma the lymphocytes were isolated using a 30%/64% Percoll gradient and centrifugation at 1,200 g, room temperature for 30 min with mild acceleration and brake. Lymphocytes were collected from the interface. In vitro lymphocytes were separated from thymocytes by overlaying onto Nycoprep. After centrifugation at 675 g, room temperature for 10 min with mild acceleration and brake, lymphocytes were collected from the interface.

Instrument

FACS VERSE (BD Biosciences), FACS Fortessa (BD Biosciences), Cytoflex S (Beckman Coulter)

Software

FACS Suite (FACS VERSE), FACSDiva (FACS Fortessa), CytExpert (Cytoflex S), FlowJO (version 10+)

Cell population abundance

Cell population abundance pre-sorting ranged from 1% to >50% depending on the tissue. Post sort, purity was confirmed by re-analysis of the sorted population.

Gating strategy

Sorting rat T cells in genome-wide and validation screening: Lymphocytes were gated in an FSC-A vs. SSC-A dot plot defined by size and granularity. Doublets were excluded in a FSC-H vs FSC-A plot. Cells in the gate were displayed in a FITC-A vs. PB450-A/BV421-A plot to identify BFP+ and GFP+ populations.

In vivo migration analysis, chemotaxis assay: Lymphocytes were gated in an FSC-A vs. SSC-A dot plot defined by size and granularity. Cells in the gate were displayed in a FITC-A (EGFP) vs. PB450-A/BV421-A (BFP) plot to identify BFP+ and GFP+ populations.

In vitro rat T cell staining: Lymphocytes were gated in an FSC-A vs. SSC-A dot plot defined by size and granularity. Doublets were excluded in a FSC-H vs FSC-A plot. Cells in the gate were displayed in a FITC-A (EGFP) vs. PB450-A/BV421-A (BFP) plot to identify BFP+ and EGFP+ populations. The populations were further displayed in a single-parameter histogram of APC-A (CD49d/CD29/CD11a/CD18/TCR/CD25/CD134)

In vitro human T cell staining: Lymphocytes were gated in an FSC vs. SSC dot plot defined by size and granularity. Doublets were excluded first in a FSC-H vs FSC-A plot second in a SSC-H vs SSC-A plot. Cells in the gate were displayed in a FITC-A (CD4) vs. PB450-A (LIVE/DEAD) plot to identify live CD4+ T cells. The populations were further displayed in a single-parameter histogram of APC-A/PE (S1PR1, CD49d / CXCR3, CD11a, CD18).

Sorting human T cells: CD3+ T cell lymphocytes were gated in a SSC vs. AF700 (CD3) plot. The gated population was further separated into CD8+ and CD4+ populations in a PerCP (CD8) vs. PacificBlue (CD4) plot. Cells in each gate were displayed in a FITC (CD45RO) vs. APC (CCR7) plot to distinguish Effector Memory cells (CD45RO+, CCR7-), Central Memory Cells (CD45RO+, CCR7+), Effector cells (CD45RO-, CCR7-) and naive cells (CD45RO-, CCR7+).

Tick this box to confirm that a figure exemplifying the gating strategy is provided in the Supplementary Information.